Glaciers determine the sensitivity of hydrological processes to perturbed climate in a large mountainous basin on the Tibetan Plateau

Yi Nan [1], Fuqiang Tian [1]

Affiliation:

1. State Key Laboratory of Hydroscience and Engineering & Department of Hydraulic Engineering, Tsinghua University, Beijing 100084, China

Corresponding to: Fuqiang Tian

Email: tianfq@tsinghua.edu.cn

Abstract

The major rivers on the Tibetan Plateau supply important freshwater resources to riparian regions, but are undergoing significant climate change in recent decades. Understanding the sensitivities of hydrological processes to climate change is important for water resource management, but large divergences exist in previous studies because of the uncertainties of hydrological models and climate projection data. Meanwhile, the spatial pattern of local hydrological sensitivities was poorly explored despite the strong heterogeneity on the Tibetan Plateau. This study adopted the climate perturbation method to analyze the hydrological sensitivities of a typical large mountainous basin (Yarlung Tsangpo River, YTR) to climate change. We utilized the tracer-aided hydrological model Tsinghua Representative Elementary Watershed-Tracer-aided version (THREW-T) to simulate the hydrological and cryospheric processes in the YTR basin. Multiple datasets and internal stations were used to validate the model, to provide confidence to the baseline simulation and the sensitivity analysis. Results indicated that: (1) The THREW-T model performed well on simulating the streamflow, snow cover area (SCA), glacier mass balance (GMB), and stream water isotope, ensuring good representation of the key cryospheric processes and a reasonable estimation of runoff components. The model performed acceptably on simulating the streamflow at eight internal stations located in the mainstream and two major tributaries, indicating that the spatial pattern

30   of hydrological processes was reflected by the model. (2) Increasing temperature led to

31   decreasing annual runoff, smaller inter-annual variation, more even intra-annual distribution,

32   and an earlier maximum runoff. It also influenced the runoff regime by increasing the

33   contributions of rainfall and glacier melt overland runoff, but decreasing the subsurface runoff

34   and snowmelt overland runoff. Increasing precipitation had the opposite effect to increasing

35   temperature. (3) The local runoff change in response to increasing temperature varied

36   significantly, with changing rate of -18.6% to 54.3% for 5℃ of warming. The glacier area ratio

37   (GAR) was the dominant factor of the spatial pattern of hydrological sensitivities to both

38   perturbed temperature and precipitation. Some regions had a non-monotonic runoff change rate

39   in response to climate perturbation, which represented the most dynamic regions within the

40   basin, as they kept shifting between energy and water limited stages. The GAR and mean annual

41   precipitation (MAP) of the non-monotonic regions had a linear relation, and formed the

42   boundary of regions with different runoff trends in the GAR-MAP plot.

43

1. Introduction

The Tibetan Plateau (TP), known as the "Asian Water Tower", is the source region of several major rivers in Asia (e.g., Yarlung Tsangpo-Brahmaputra Lantsang-Mekong, Indus, Ganges). The contributions of runoff in the source regions of TP rivers to the total runoff in whole basins range from 6%-60% (Tang et al., 2019; Wang et al., 2020; Cao and Pan, 2014), sustaining the ecosystems and supplying valuable freshwater resources for downstream livelihoods (Immerzeel et al., 2010; Lutz et al., 2014). The sustainable socioeconomic development and the decision-making of water resource management in the riparian countries around the TP rely heavily on the runoff in the major river basins (Cui et al., 2023). Meanwhile, the TP is a typical high mountainous cryosphere, characterized by large stores of frozen soil and frequent multiphase water transferring, resulting in complex hydrological processes and multiple water sources including rainfall, snowmelt and glacier melt (Li et al., 2019; Yao et al., 2022). The melting processes of frozen water are determined by energy budget, and the runoff change on the TP is extremely sensitive to climate change (Gao et al., 2019). Consequently, understanding hydrological processes and estimating the runoff change on the TP is not only of great practical significance, but also a frontier scientific question in global change.

The TP is undergoing significant climate change in recent decades, with a warming rate twice the global average level (Yao, 2019). Based on the recently released Coupled Model Intercomparison Project Phase 6 (CMIP6) (Eyring et al., 2016), the warming levels of 1.5°C, 2°C and 3°C over the TP will be attained around the 2030s, 2050s and 2070s, respectively, and the precipitation is also likely to increase significantly (Cui et al., 2023). The hydrological cycling and water resources will change correspondingly; thus it is important to understand the hydrological processes on the TP and the hydrological response to climate change. Plenty of studies have adopted hydrological models to project the runoff change on the TP in the future, but the reported trends and changing rates varied considerably in existing studies. Wang et al. (2021) and Lutz et al. (2014) projected an increasing runoff trend till the end of 21st century, while Cui et al. (2023) predicted the runoff to decrease before the 2030s and turn over to an increasing trend after that. A primary reason for the divergence in existing studies is the model uncertainties. The parameters are usually inadequately constrained solely by the streamflow observation data because of the complex hydrological processes, resulting in large uncertainties

74   in the estimation on the contributions of runoff components (Tian et al., 2020; Nan et al., 2021a),

75   which influence the runoff projection significantly. For instance, Lutz et al. (2014) estimated

76   the contribution of glacier melt to annual runoff as 0.86~40.59% in the major TP rivers,

77   resulting in an increasing runoff with climate warming, while Cui et al. (2023) estimated the

78   contribution as 0.73~14.33% and resulting in a decreasing trend in the near future. Nonetheless,

79   recently developed hydrological models integrating key cryospheric processes (e.g., Cui et al.,

80   2023) have been proved as effective tools for hydrological simulations on the TP, and the high-

81   quality datasets of snow and glacier (e.g., Chen et al., 2018; Hugonnet et al., 2022) can provide

82   adequate validation for the corresponding models. Moreover, tracer-aided hydrological models

83   integrating modules of tracer storage, mixture, and transportation processes forced by the

84   outputs of isotopic general circulation models (iGCMs) have proved to constrain the

85   hydrological model uncertainties significantly (He et al., 2019; Birkel and Soulsby, 2015;

86   Stadnyk and Holmes, 2023), especially for the separation of runoff components (Nan et al.,

87   2021a, 2023). These developments of models and datasets bear the potential to provide a more

88   reasonable baseline for streamflow projection.

89   Another major source of runoff projection uncertainty is the uncertainty of climatic forcing

90   data (Li et al., 2014). The climatic data in the future are generally generated by the general

91   circulation models (GCMs), which cannot be directly adopted in the catchment scale because

92   of the insufficient spatial resolution and accuracy, so downscaling and bias correction are

93   necessary steps in using GCM data at regional scale (Xu et al., 2019; Olsson et al., 2015).

94   However, even being corrected by the observation data during the historical period, the

95   divergence among the outputs of different GCMs is still significant. For example, the difference

96   in the precipitation change over the TP among 22 CMIP6 products could be larger than 50%

97   (Cui et al., 2023). Bloschl and Montanari (2010) pointed out the large uncertainties of studies

98   analyzing the impact of climate change, and compared them to throwing a dice. As an

99   alternative method, producing hypothesized climate change scenarios by perturbing the current

100 temperature and precipitation data has proved to be valuable in investigating the hydrological

101 sensitivities to climate change (Ayguen et al., 2020; Rasouli et al., 2015; He et al., 2021b). The

102 range of climate perturbation is assumed based on the possible change range projected by an

103 ensemble of GCMs, providing a possible runoff change range accordingly (Su et al., 2023; He

104 et al., 2021b). The climate perturbation method also allows for a deeper analysis of the separate

105 effect of each climatic factor and the compensation effects among them (He and Pomeroy,

106 2023).

107 Although plenty of studies have been conducted for the TP rivers to project the runoff

108 change or analyze the hydrological sensitivities to climate change, most of them were

109 conducted at the regional or basin scale (e.g., Su et al., 2023; Zhang et al., 2022b). The local

110 hydrological response to climate change could significantly differ among small catchments due

111 to the different geographical and meteorological characteristics (Bai et al., 2023), which is

112 important for local water resources utilization and management (Zhang et al., 2015).

113 Considering the strong heterogeneity in meteorological factors and land surface conditions in

114 the large river basins on the TP (Wang et al., 2021; Li et al., 2020), the local hydrological

115 sensitivities to climate change should have strong variability over the TP. However, the spatial

116 pattern and influence factors of the local hydrological sensitivities within the basin are poorly

117 explored, partly due to the scarce hydrological stations for model validation, resulting in a lack

118 of confidence in the spatial representation of hydrological processes.

119 Motivated by the mentioned background, this study utilized the spatially distributed tracer-

120 aided hydrological model THREW-T developed by Nan et al. (2021b) in the Yarlung Tsangpo

121 River basin, a typical large mountainous basin on the Tibetan Plateau, to explore its

122 hydrological sensitivity to perturbed temperature and precipitation. Snow, glacier, isotope data

123 and observation streamflow at nine stations were collected to validate the model. The spatial

124 pattern of the local hydrological sensitivities and the influence factors were analyzed in

125 particular. The main objectives of this study are as follows: (1) to test the performance of

126 THREW-T model on simulating all the hydrological and cryospheric processes in the Yarlung

127 Tsangpo River basin, (2) to analyze the sensitivities of hydrological processes in the Yarlung

128 Tsangpo River basin to a reasonable range of perturbed temperature and precipitation, and (3)

129 to analyze the spatial pattern and the influence factors of the local hydrological sensitivities.

130 **2. Data and methodology**

131 **2.1 Study area**

132 This study focused on the Yarlung Tsangpo River (YTR) basin, the upstream part of the

Brahmaputra River basin, located in the southern TP (Figure 1). The YTR is one of the longest rivers originating from the TP (longer than 2000 km), extending in the range of 27~32°N and 82~97°E with an elevation extent of 2900~6900 m a.s.l. (above sea level). The mean annual precipitation and temperature in the YTR basin are around 500 mm and -0.2 °C, respectively. The YTR has four major tributaries, i.e., DoxungZangbo, Nianchu River, Lhasa River, and Nyang River, from upstream to downstream. The precipitation is dominated by the South Asian monsoon in the Indian Ocean hydrosphere-atmosphere system, resulting in an obviously wet season from June to September. The outlet hydrological station along the mainstream is the Nuxia station, above which the drainage area is approximately 2×10^5 km^2, and around 1.5% is covered by glaciers.
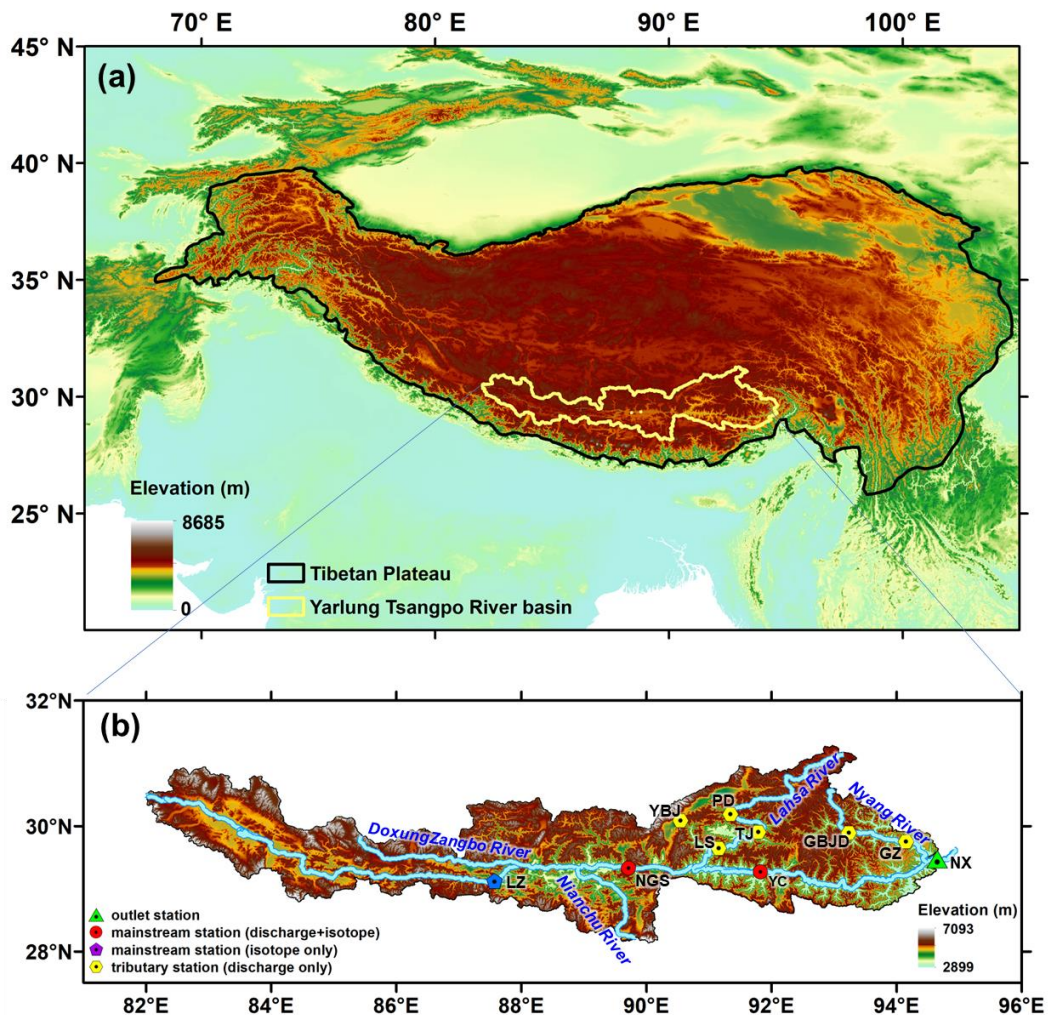
Figure 1. Locations and topography of (a) the Tibetan Plateau and (b) the Yarlung Tsangpo River basin. The stations used for model validation are shown in Figure (b). The abbreviations

146   NX, YC, NGS, LZ, GZ, GBJD, LS, TJ, PD and YBJ represent Nuxia, Yangcun, Nugesha, Lazi,

147   Gengzhang, Gongbujiangda, Lahsa, Tangjia, Pangduo and Yangbajing stations, respectively.

148   **2.2 Data**

149   The 30 m resolution digital elevation model (DEM) data for the YTR basin was extracted

150   from the Geospatial Data Cloud (https://www.gscloud.cn). Daily precipitation, temperature,

151   and potential evapotranspiration data were extracted from the China Meteorological Forcing

152   Dataset (CMFD, Yang and He, 2019) with 0.1° resolution. For the cryospheric processes, the

153   Tibetan Plateau Snow Cover Extent (TPSCE) product (Chen et al., 2018) and the second glacier

154   inventory dataset of China (Liu, 2012) were adopted to denote the snow and glacier coverage.

155   The yearly glacier elevation change data with 0.5° resolution developed by Hugonnet et al.

156   (2021) was used to represent the glacier mass balance. For the underlying conditions, the

157   MODIS leaf area index (LAI) product MOD15A2H (Myneni et al., 2015) and normalized

158   difference vegetation index (NDVI) product MOD13A3 (Didan, 2015) were adopted to

159   represent the vegetation coverages, and the Harmonized World Soil Database (HWSD, He,

160   2019) was used to estimate the soil property parameters. Daily streamflow data at nine stations

161   were collected (Figure 1 and Table 1).

162   **Table 1**. The name, location and data period of the hydrological stations

Station	Mainstream/tributary	Period
Nuxia	Mainstream	1991~2015
Yangcun	Mainstream	2001~2010
Nugesha	Mainstream	2001~2010
Gengzhang	Nyang river	2001~2015
Lhasa	Lhasa river	2001~2015
Gongbujiangda	Nyang river	2006~2009, wet season
Yangbajing	Lhasa river	2006~2015, wet season
Pangduo	Lhasa river	2001~2015, wet season
Tangjia	Lhasa river	2001~2015, wet season

163   Grab samples of precipitation and stream water were collected in 2005 at four stations

164   along the mainstream of YTR, i.e., Lazi, Nugesha, Yangcun, and Nuxia, from upstream to

165   downstream, for isotope analysis (Table 2, Liu et al., 2007). The outputs of Scripps Global

166   Spectral Model with isotope incorporated (isoGSM, Yoshimura et al., 2008) with 1.875°

167   resolution were extracted to represent the spatiotemporal variation of precipitation isotope in

168   the YTR basin. According to our previous assessment based on the measurement precipitation

7

169 isotope data, the isoGSM captured the seasonality of precipitation isotope well, but had

170 systematic overestimation biases in the YTR basin, which were highly correlated to the altitude

171 (Nan et al., 2021a). The corrected isoGSM in the YTR basin produced by Nan et al. (2022) was

172 adopted in this study.

173 **Table 2.** Summary of measurement isotope data in the YTR basin during 2005

Station	Period	Precipitation			Stream		
		Number of samples	$\overline{\delta^{18}O}$ (‰)	SD (‰)	Number of samples	$\overline{\delta^{18}O}$ (‰)	SD (‰)
Nuxia	14 Mar. – 23 Oct.	86	-10.33	7.18	34	-15.74	1.60
Yangcun	17 Mar. – 5 Oct.	59	-13.17	7.10	30	-16.57	1.69
Nugesha	14 May. – 22 Oct.	45	-14.29	7.99	25	-17.84	0.99
Lazi	6 Jun. – 22 Sep.	42	-17.41	5.75	22	-16.52	1.43

174 **2.3 The tracer-aided hydrological model**

175 A distributed tracer-aided hydrological model, Tsinghua Representative Elementary

176 Watershed-Tracer-aided version (THREW-T) model, developed by Tian et al. (2006) and Nan

177 et al. (2021b), was adopted to simulate the hydrological and isotopic processes in the YTR basin.

178 The model uses the representative elementary watershed (REW) method for spatial

179 discretization of basins, dividing the whole catchment into REWs based on DEM data. Each

180 REW is further divided into two vertically distributed layers (i.e., surface and subsurface layers),

181 including eight subzones (i.e., surface layer: vegetation zone, bare zone, main channel reach

182 zone, sub stream network zone, snow-covered zone, and glacier-covered zone; subsurface layer:

183 unsaturated zone and saturated zone) (Reggiani et al., 1999; Tian et al., 2006). This study

184 divided the YTR basin into 297 REWs, with an average area of 694 km^2, ranging from 162 to

185 2753 km^2. More model details are provided in Tian et al. (2006).

186 A cryospheric module representing the evolutions of snowpack and glacier was

187 incorporated into the model for application in cold regions. The total precipitation was

188 partitioned into liquid and solid precipitation according to a temperature threshold, which was

189 set as 0°C. The degree-day factor method was used to calculate the meltwater. The snow water

190 equivalent of each REW was updated based on the snowfall (i.e., the solid precipitation) and

191 the snowmelt, and the snow cover area was then determined by the snow cover depletion curve

192 (Fassnacht et al., 2016). To simulate the evolution of glaciers, each REW is further divided into

several elevation bands to represent the change in temperature and precipitation along the altitudinal profile. The glacier within the intersection of each REW and elevation band is regarded as the representative unit for glacier simulation, similar to the discretization strategy adopted by Luo et al. (2013). For each glacier simulation unit, the model simulates the processes including the accumulation and melt of snow over glacier, the turnover of snow to ice, and the ice melt. More details and equations of the cryospheric module are provided in Nan et al. (2021b) and Cui et al. (2023).

The tracer module was incorporated into the model to simulate the isotope composition of multiple water bodies. The Rayleigh equation was adopted to simulate the isotope fractionation during water evaporation and snowmelt processes (He et al., 2019; Hindshaw et al., 2011). The isotope composition of glacier meltwater was assumed to be constantly more depleted than the local precipitation isotope and was estimated by an offset parameter (Nan et al., 2022). The isotope compositions in each simulation unit were calculated based on the complete mixing assumption. The isotope composition of snowpack and snowmelt was updated based on the water and isotope mass balance of the snowpack, similarly with other water storages. Forced by the precipitation isotope composition, the model can simulate the isotope composition of all water bodies, including stream water, soil water, groundwater, and snowpack. More details and calculation equations of the tracer module are provided in Nan et al. (2021b).

The THREW-T model quantified the contributions of multiple runoff components based on the flow-pathway definition as reviewed by He et al. (2021a). The runoff was firstly divided into surface runoff and subsurface runoff (baseflow) based on the runoff generation pathway. The surface runoff was then further divided into three components induced by different water sources (rainfall, snowmelt, and glacier melt). As a result, the total runoff was divided into four components: subsurface runoff, rainfall overland runoff, snowmelt overland runoff, and glacier melt overland runoff.

2.4 Model calibration and evaluation

The model was run for 25 years starting from 1991 to 2015, and was calibrated toward four objectives: the discharge at Nuxia station from 2001 to 2015, the snow cover area (SCA) from 2001 to 2015, the average glacier mass balance (GMB) from 2001 to 2010 in the whole

YTR basin, and the stream water isotope at the four stations in 2005. The Nash-Sutcliffe efficiency (NSE) was set as the evaluation metric for objectives with strong seasonality (discharge and isotope), and the root mean square error (RMSE) was set as the evaluation metric for objectives with essentially fluctuations (SCA and GMB) (Schaefli and Gupta, 2007). The optimization objective function of calibration procedure was calculated by combining the function of each objective with equal weights.

An automatic algorithm, the Python Surrogate Optimization Toolbox (pySOT, Eriksson et al., 2019) were adopted for model calibration. The pySOT algorithm uses radial basis functions (RBFs) as surrogate models to approximate the simulations, reducing the time for each model run. The symmetric Latin hypercube design (SLHD) method was used to generate parameter values, allowing an arbitrary number of design points. In each optimization run, the procedure stopped when a maximum number of allowed function evaluations was reached, which was set as 3000. In this study, the pySOT algorithm was repeated for 100 times, and a final parameter set was selected from the calibrated parameter sets manually based on the overall performance on multiple objectives. The physical basis, reference ranges and calibrated values of the calibrated parameters in the THREW-T model are shown in Table 3.

Apart from the calibration functions, the model performances were additionally evaluated by four statistical metrics: logarithmic NSE (lnNSE), RMSE-observations standard deviation ratio (RSR), Percent bias (PBIAS) and correlation coefficient (CC). The discharge simulation was evaluated by lnNSE to examine the simulation of baseflow process. Our previous studies indicated that the discharge simulation performance during validation was highly correlated with that of calibration period, partly due to the strong linearity of precipitation-discharge relation in such a large basin, but large uncertainties existed in the discharge simulation at internal stations even when the discharge at outlet station was simulated well (Nan et al., 2021b, 2022). Consequently, we not only conducted temporal validation based on the discharge data at Nuxia station during 1991~2000, but also collected additional discharge data at eight internal stations to assess the spatial consistency of model performance. The RMSE and CC of the cumulative glacier mass balance since the beginning of simulation period were also calculated to assess the glacier simulation, considering the temporal interpolation adopted by Hugonnet et al. (2021) which led to uncertainty in the year scale data.

$$252 \quad \text{NSE} = 1 - \frac{\sum(X_\text{o} - X_\text{S})^2}{\sum(X_\text{o} - \overline{X_\text{o}})^2} \tag{1}$$

$$253 \quad \text{lnNSE} = 1 - \frac{\sum(\ln(X_\text{o}) - \ln(X_\text{S}))^2}{\sum(\ln(X_\text{o}) - \overline{\ln(X_\text{o})})^2} \tag{2}$$

$$254 \quad \text{RMSE} = \sqrt{\frac{\sum(X_\text{o} - X_\text{S})^2}{n}} \tag{3}$$

$$255 \quad \text{RSR} = \frac{\text{RMSE}}{\text{STD}_\text{obs}} = \frac{\sqrt{\sum(X_\text{o} - X_\text{S})^2}}{\sqrt{\sum(X_\text{o} - \overline{X_\text{o}})^2}} \tag{4}$$

$$256 \quad \text{PBIAS} = \frac{\sum(X_\text{o} - X_\text{S}) * 100}{\sum X_\text{o}} \tag{5}$$

$$257 \quad \text{CC} = \frac{\sum[(X_\text{S} - \overline{X_\text{S}})(X_\text{o} - \overline{X_\text{o}})]}{\sqrt{\sum[(X_\text{S} - \overline{X_\text{S}})^2(X_\text{o} - \overline{X_\text{o}})^2]}} \tag{6}$$

258 where, X_s, X_o, $\overline{X_\text{S}}$ and $\overline{X_\text{o}}$ are the simulated, observed, mean of simulated and mean of

259 observed hydrological variables, respectively, and n is the number of data.

260 **Table 3.** Physical descriptions, reference ranges and calibrated values of the calibrated

261 parameters in the THREW-T model

Symbol	Unit	Description	Reference range	Calibrated value
WM	cm	Tension water storage capacity used to calculate the saturation area	0~10	2.92
B	-	Shape coefficient used to calculate the saturation area	0~1	0.04
KKA	-	Exponential coefficient to calculate the subsurface runoff outflow rate	0~6	5.92
KKD	-	Linear coefficient to calculate the subsurface runoff outflow rate	0~0.5	0.21
DDF$_\text{S}$	Mm/°C/d	Degree day factor for snowmelt	0~10	2.60
DDF$_\text{G}$	Mm/°C/d	Degree day factor for glacier melt	0~10	1.51
T$_0$	°C	Temperature threshold above which snow and glaciers melting occurs	-5 ~ 5	-4.28
C$_1$	-	Coefficient to calculate concentration process using the Muskingum method	0~1	0.04
C$_2$	-	Coefficient to calculate concentration process using the Muskingum method	0~1	0.80

262 **2.5 Perturbed climatic scenarios design**

263 Daily temperature and precipitation data extracted from the CMFD dataset were set as the

264 reference climate inputs. Linearly perturbed temperature and precipitation time series were

265 adopted to represent the potential climate change ranges. Perturbed temperature input data was

266 generated by adding one-degree increments to the reference daily temperature. The maximum

11

temperature increase was set as 5 °C, because the temperature in the YTR basin is projected to increase at 1°C/20 yrs, and will increase by about 5 °C until the end of this decade (Cui et al., 2023). The influence of changing temperature on the potential evapotranspiration was estimated by the regression between the two factors (Eq. 7) which was developed by Van Pelt et al. (2009) and widely adopted in the projection of potential evapotranspiration (e.g., Xu et al., 2019; Cui et al., 2023).

$$E_p = [1 - \alpha_0(T - \overline{T_0})] \cdot \overline{E_{p0}} \tag{7}$$

where, $\overline{T_0}$ and $\overline{E_{p0}}$ are the mean daily temperature and potential evapotranspiration in each REW during the simulation period, respectively. T is the daily temperature generated by the perturbation method. α_0 is determined by regressing the input daily potential evapotranspiration and temperature in each REW.

Perturbed precipitation input data was generated by multiplying the reference daily precipitation data from 80% to 120% with an increment of 10%, similar to Su et al. (2023) which analyzed the runoff change of three basins on the TP under hypothesized climate change scenarios. Simulation during 2001~2015 was set as the reference scenario, because the data of most objectives/stations were available during this period. In total, one reference simulation, five simulations of perturbed temperature and four simulations of perturbed precipitation were conducted. To focus on the influence of climate perturbations on the hydrological processes, the changes of underlying conditions such as soil and vegetation were not considered. In each scenario, the standard deviations (STD) of the simulated annual hydrological variables were calculated to represent the uncertainties introduced by natural climate variability. The t-Test analysis of paired two samples was conducted for the annual hydrological variables produced by reference scenario and each climate perturbation scenarios, to analyze the statistical significance of the changes. Apart from the basic hydrological variables, the concentration ratio (CR) and concentration period (CP) (Jiang et al., 2022a) were calculated by Eqs. 8~10 to characterize the runoff seasonality.

$$CR = \sqrt{R_x^2 + R_y^2} / \sum_{i=1}^{12} R_i \tag{8}$$

$$CP = \arctan(R_x/R_y) \tag{9}$$

$$R_x = \sum_{i=1}^{12} R_i \times \sin(\theta_i); \quad R_y = \sum_{i=1}^{12} R_i \times \cos(\theta_i) \tag{10}$$

296   where, R_i is the runoff in the *i*th month, R_x and R_y are the resulting vectors in the direction of *x*

297   and *y*, respectively. $\theta_i=360°/12×i=30°×i$ (*i*=1,2,…,12).

298   **3. Results**

299   **3.1 Model performance evaluation**

300   Figure 2 shows the model performances on the four calibration objectives. The discharge

301   was simulated well regarding both high flow and baseflow processes, as indicated by the high

302   NSE (0.82) and lnNSE (0.84). The occurring times of peak flow were captured by the model,

303   showing the consistency in the temporal dynamics of simulated and observed streamflow, but

304   the simulated magnitudes of peak flow were slightly lower than the observation (Figure 2a),

305   partly due to the poor abilities of precipitation products on accurately capturing the high

306   precipitation in high elevation elevations and the amount of specific precipitation extreme

307   events (Li et al., 2021; Jiang et al., 2022b; Xu et al., 2017). The performance of discharge

308   simulation during validation period was similar with that of calibration period, with NSE and

309   lnNSE of 0.80 and 0.88 respectively, as shown in Figure 2a. Nonetheless, the simulated annual

310   runoff (302 mm/yr) was very close to the observation (303 mm/yr), indicating that the amount

311   of total runoff was reproduced well. The simulated variation of SCA was smoother than the

312   observation, but the seasonality was captured well, i.e., decreasing sharply in May and

313   remaining extremely low from July to September (Figure 2b). The low RMSE (<0.1) suggested

314   that the model performed well on simulating the snow processes. The model successfully

315   simulated the declining glacier (Figure 2c), with an extremely high CC for the cumulative

316   glacier mass balance (~1). The model estimated the annual GMB in the YTR basin as -0.545

317   m/yr, very close to the value extracted from the dataset of Hugonnet et al. (2021) (-0.554 m/yr).

318   The calibrated melting temperature threshold was rather low (-4.28℃), which was partly due

319   to the fact that melting processes were simulated at the daily step. The model simulated the

320   variation of stream isotope well, indicated by the high NSE, CC and low PBIAS, which

321   provided confidence in the partitioning among different runoff components (Nan et al., 2021a;

322   He et al., 2019). The seasonality of the isotope was adequately captured: getting enriched in

323   May, reaching maximum in June, and getting depleted in late June/early July (Figure 2d). The

324   fact that the model simultaneously satisfied four calibration objectives ensured the proper

325   representation of the hydrological and cryospheric processes, and provided a reasonable

326   baseline for the sensitivity analysis.
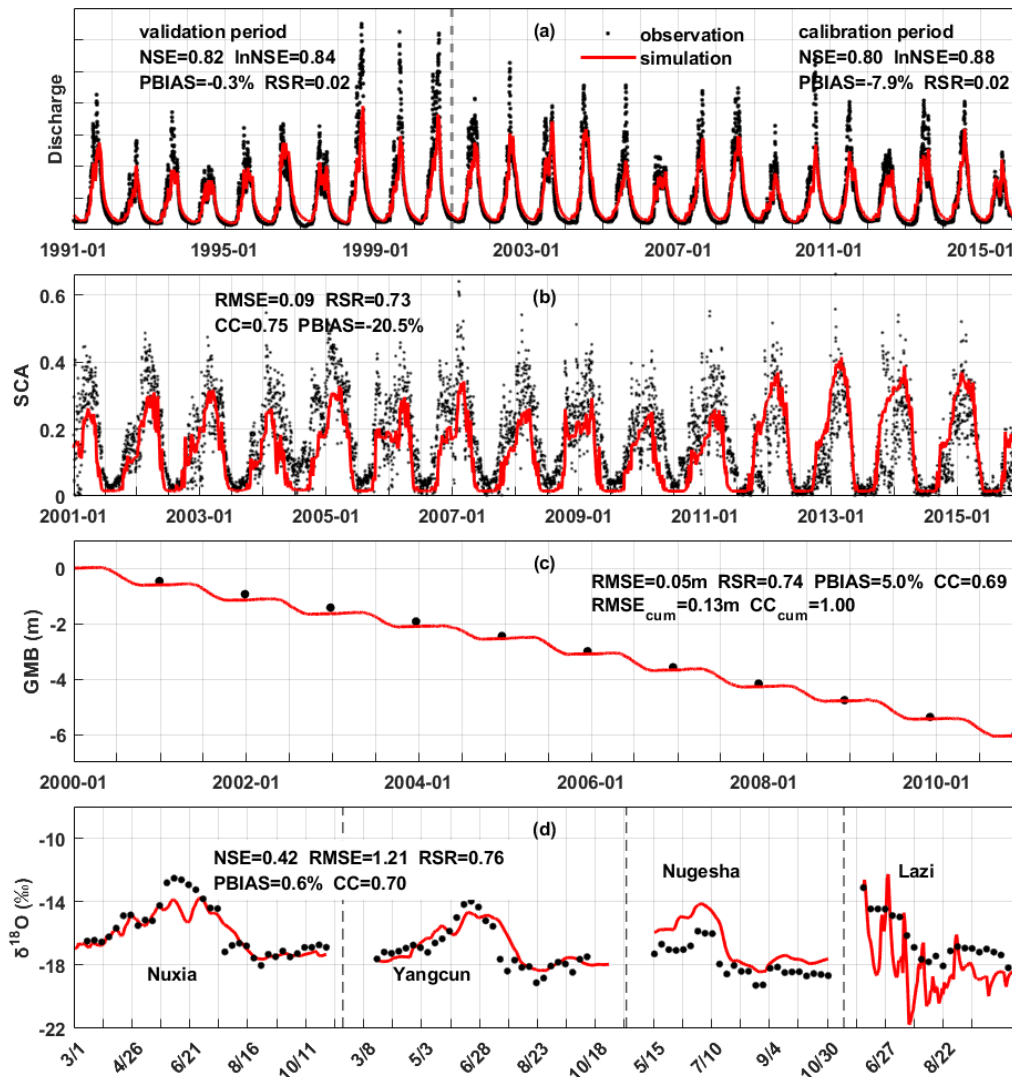
327

328   **Figure 2.** The model performances on the calibration objectives. (a) the streamflow discharge

329   at Nuxia station, (b) the snow cover area ratio in the YTR basin, (c) the average glacier mass

330   balance in the YTR basin, and (d) the stream water isotope at four stations in 2005.

331   Figure 3 shows the streamflow simulation at eight internal stations. The performance

332   ratings were evaluated based on four metrics following the guideline by Moriasi et al. (2007).

333   At the two stations located along the mainstream (Yangcun and Nugesha), the high flow

334   processes were simulated well as indicated by the high NSE, but the baseflows were

335   overestimated (Figure 3a and b). In contrast, the high flow processes were underestimated at

336   Gengzhang station, but the baseflows were reproduced well (Figure 3c). The model produced

337   fair performance on both high flow and baseflow simulation at Lhasa station, showing moderate

NSE and lnNSE (Figure 3d). For the four stations where only the data during the wet season were available, the PBIASs were at good levels (within $\pm 15\%$) except for Gongbujiangda station (Figure 3e-h). Overall, the streamflow simulations at internal stations were not as good as the calibrated outlet station, but were at acceptable levels, as indicated by at least one satisfactory metric except for Gongbujiangda station. The high flow processes and runoff amount were reproduced relatively well, as indicated by the generally satisfactory NSE and PBIAS. But the small time-scale fluctuations and extremes were mostly not captured well, because the model was not evaluated toward metrics related to hydrological signatures (McMillan et al., 2017; Majone et al., 2022; Fenicia et al., 2018). Nonetheless, the validation based on the internal stations gave confidence in the spatial pattern of the hydrological processes and their sensitivities to the perturbed climate.
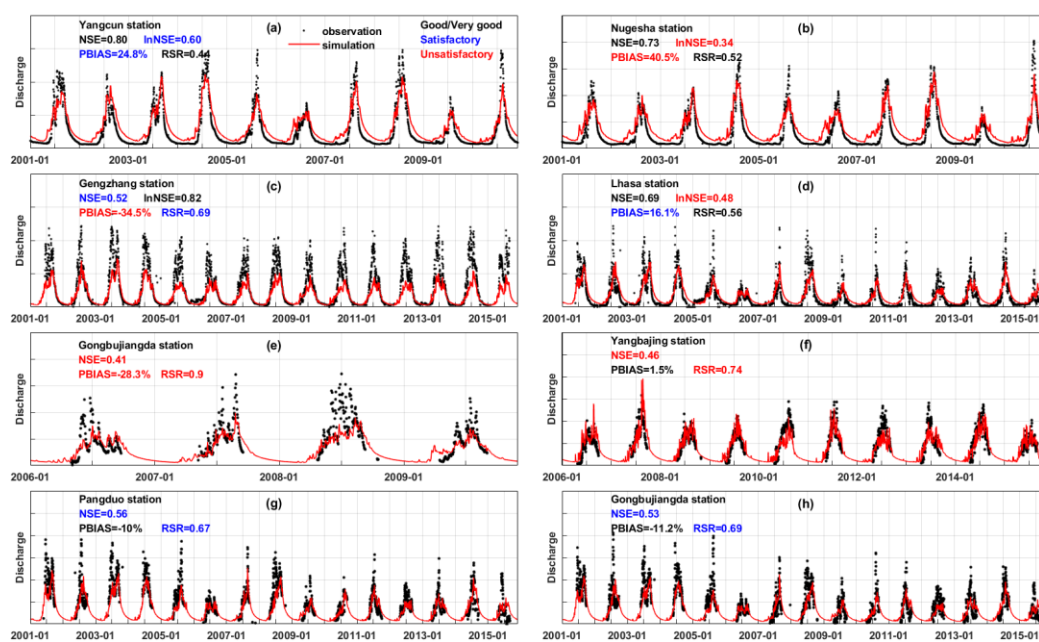

Figure 3. The model performances on the streamflow simulation at the internal stations.

3.2 Sensitivities of hydrological variables to perturbed temperature and precipitation

The sensitivities of annual runoff, snow cover area, and glacier mass balance to perturbed temperature and precipitation are shown in Figure 4. The relationships between hydrological variables and precipitation/temperature showed strong linearity, which was similar with Su et al. (2023) analyzing the hydrological sensitivities in three other large basins on the TP ($\sim 10^5$ km^2), but was different from He et al. (2021b) which conducted a similar analysis in a small boreal forest basin in Canada (603 km^2). The annual runoff kept decreasing significantly with

15

the increasing temperature at the rate of -2 mm/°C due to the increasing evaporation (Figure

4a). The decreasing rate got small when the temperature increase was higher than 3°C, partly

because the controlling factor of evaporation changed from energy limitation to water limitation

(Wang et al., 2022). The runoff change in response to increasing temperature was rather small

compared to the intra-annual runoff variability. The snow cover area ratio significantly reduced

with the increasing temperature at the rate of -1.5%/°C because of the decreasing snowfall and

increasing snowmelt, and would be smaller than half of the reference scenario for 5°C of

warming (Figure 4b). The glacier mass balance significantly got more negative with the

increasing temperature because of the reducing accumulation and increasing meltwater, at the

rate of -0.16 m/°C (Figure 4c). Among the three variables, the glacier mass balance was the

most sensitive to the warming climate, the relative change of which could be 150% for 5°C of

warming (Figure 4d). The changes of runoff, snow cover area and glacier mass balance in

response to increasing temperature were all statistically significant at 0.01 significance level.
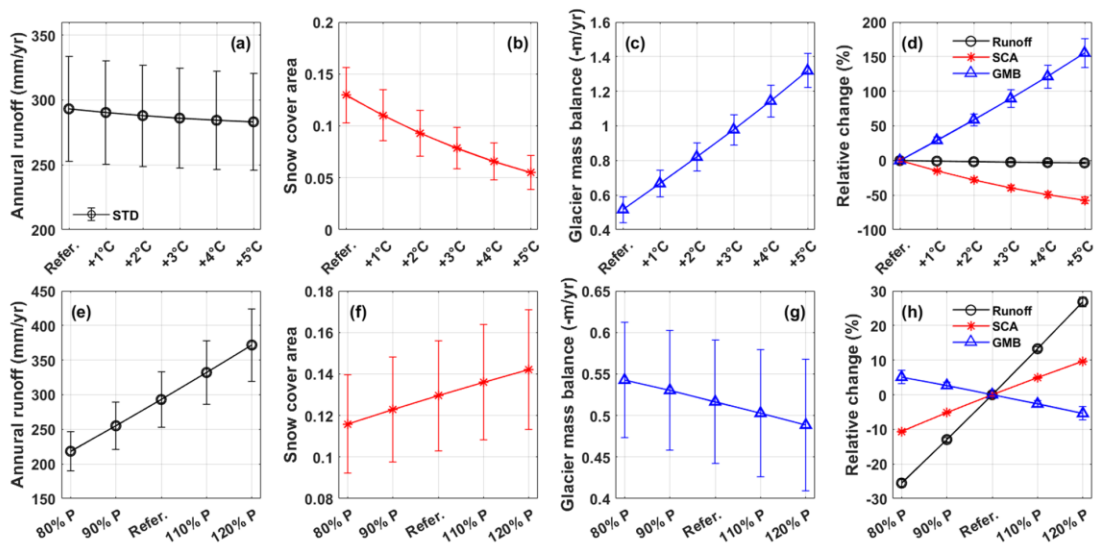
Figure 4. The sensitivities of annual runoff, snow cover area, and glacier mass balance to the

perturbed temperature (a-d) and precipitation (e-g). Subplots (d) and (h) are the relative changes

of runoff, SCA and GMB compared to the reference scenario.

The hydrological sensitivities to perturbed precipitation were opposite to that of

temperature. The annual runoff increased at the rate of 38.4 mm/10% with the increasing

precipitation (Figure 4e). The relative change in runoff was larger than precipitation (Figure

4h), indicating an increasing runoff coefficient with increasing precipitation. This also indicated

379 a small relative change in evaporation in response to precipitation perturbation, again

380 suggesting that the energy limitation played more important role than water limitation on

381 evaporation in the reference scenario. With the increasing precipitation, the snow cover area

382 increased at 0.7%/10%, and the glacier mass balance got more positive at 0.014m/10% because

383 of the larger amount of snowfall and snow/ice accumulation (Figure 4f and 4g). Among the

384 three variables, the runoff had the highest sensitivity to perturbed precipitation, with a relative

385 change rate of 13%/10% (Figure 4h), while the changes of snow cover area and glacier mass

386 balance were within the range of ±10% when precipitation changed by 20%. The changes of

387 runoff, snow cover area and glacier mass balance in response to perturbed precipitation were

388 all statistically significant at 0.01 significance level.

389 **3.3 Sensitivities of runoff variation to perturbed temperature and precipitation**

390 The sensitivities of inter- and intra-annual runoff variation to perturbed temperature and

391 precipitation are shown in Figure 5. The average monthly runoff were calculated based on the

392 simulated hydrographs during the entire simulation period, and the inter-annual runoff variation

393 was represented by the STD. The change of inter-annual runoff variation was consistent with

394 that of total runoff. The inter-annual runoff variations were also lower in the scenarios with less

395 runoff (increasing temperature or decreasing precipitation), showing the narrower ranges of the

396 error bars in Figure 5a-b, and vice versa. Despite the decreasing runoff caused by increasing

397 temperature, the average runoff for 5°C of warming was still much higher than the lower error

398 bar of the reference scenario (Figure 5a), suggesting that the runoff change tendency caused by

399 the increasing temperature was relatively small compared to the inherent runoff variability. On

400 the contrary, when precipitation increased by 20%, the average annual runoff was higher than

401 the runoff in wet years of reference scenario (Figure 5b), indicating that the trend of

402 precipitation change had a larger influence on the runoff than the inter-annual variation of

403 precipitation.

404
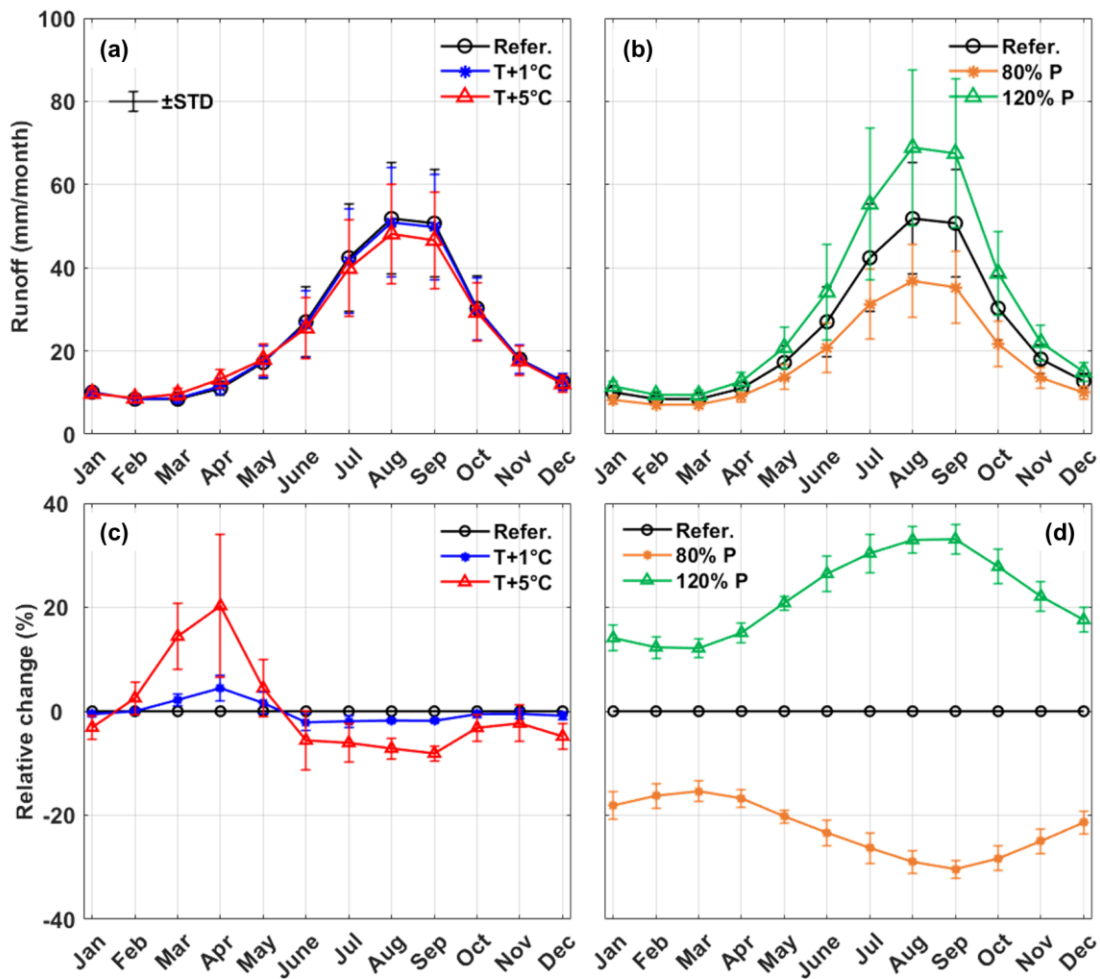
Figure 5. Sensitivities of intra- and inter-annual streamflow variability to the perturbed temperature and precipitation. (a) and (b) monthly runoff, (c) and (d) relative change of monthly runoff.

The sensitivities of monthly runoff were different among months. Although increasing temperature led to a decrease in the total runoff, it caused an increasing spring runoff. The monthly runoff in April increased most significantly, which increased 20% for 5°C of warming (Figure 5e). This could be attributed to the increasing snowmelt, because the SCA decreased significantly during the same period (Figure 2b). The monthly runoff in all twelve months changed accordingly to perturbed precipitation, but the change during wet seasons (August to October) was the most significant (Figure 5f). The different monthly runoff sensitivities in response to perturbed temperature and precipitation indicated that temperature changes influenced more on baseflow, while precipitation changes had higher impact on high flow processes. As a result, increasing temperature caused a more even distribution of monthly

runoff, while increasing precipitation had the opposite effect. The CR decreased from 0.432±0.044 to 0.402±0.046 for the warming of 5℃, indicating a more even seasonal runoff distribution caused by increasing temperature. The CP decreased by around two days, indicating that climate warming would result in advance of maximum runoff. The STD of CP slightly increased from 7.09 days at the reference scenario to 7.45 days for the warming of 5℃. On the contrary, the CR changed from 0.398±0.039 to 0.465±0.045 when precipitation increased from 80% to 120% of the reference, indicating that increasing precipitation made the distribution of runoff more concentrated. The CP advanced by 2.2 days in response to a 20% decreasing precipitation, but only recessed by 0.3 days in response to an increasing precipitation with the same magnitude. Similar with the response to warming temperature, the STD of CP also slightly increased in response to increasing precipitation. The change of CR was significant at significance level of 0.01 in all scenarios, but the change of CP was insignificant in some scenarios, including T +1℃, 110% P and 120% P, with p value of 0.014, 0.02 and 0.12, respectively.

Table 4. The concentration ratio (CR) and concentration period (CP) of runoff in different scenarios with perturbed temperature and precipitation

		CR		CP (days)	
		Average	STD	Average	STD
Reference scenario		0.432	0.044	244.4	7.09
T scenario	+1℃	0.425	0.044	244.1	7.12
	+2℃	0.419	0.045	243.8	7.18
	+3℃	0.413	0.045	243.3	7.26
	+4℃	0.408	0.046	242.8	7.36
	+5℃	0.402	0.046	242.3	7.45
P scenario	80%	0.398	0.039	242.2	6.86
	90%	0.415	0.042	243.6	7.01
	110%	0.449	0.045	244.7	7.13
	120%	0.465	0.045	244.7	7.14

3.4 Sensitivies of runoff components to perturbed temperature and precipitation

The contributions of runoff components in the YTR basin under scenarios with different temperature and precipitation are shown in Figure 6. In the reference scenario, the subsurface runoff was the dominant component, contributing 67.8±1.7% to the total runoff. Among the three surface runoff components, rainfall was the dominant water source contributing 21.6±1.3%

19

to the total runoff. Glacier melt overland runoff had considerable contribution to the runoff which contributed 7.4±1.4% to the total runoff, while the contribution of snowmelt overland runoff was only 3.2±0.9%. The annual subsurface runoff was 195.8±31.0 mm/yr (39.2±6.2 km^3/yr), close to the amount (30 km^3/yr) estimated by Yao et al. (2021) with the groundwater model MODFLOW. It should be noted that in our model all the glacier meltwater was assumed to generate surface runoff directly because of the impermeable glacier surface, while the snowmelt was assumed to be partitioned into two components (infiltration and surface runoff) (Nan et al., 2021b, 2023; Schaefli et al., 2005).
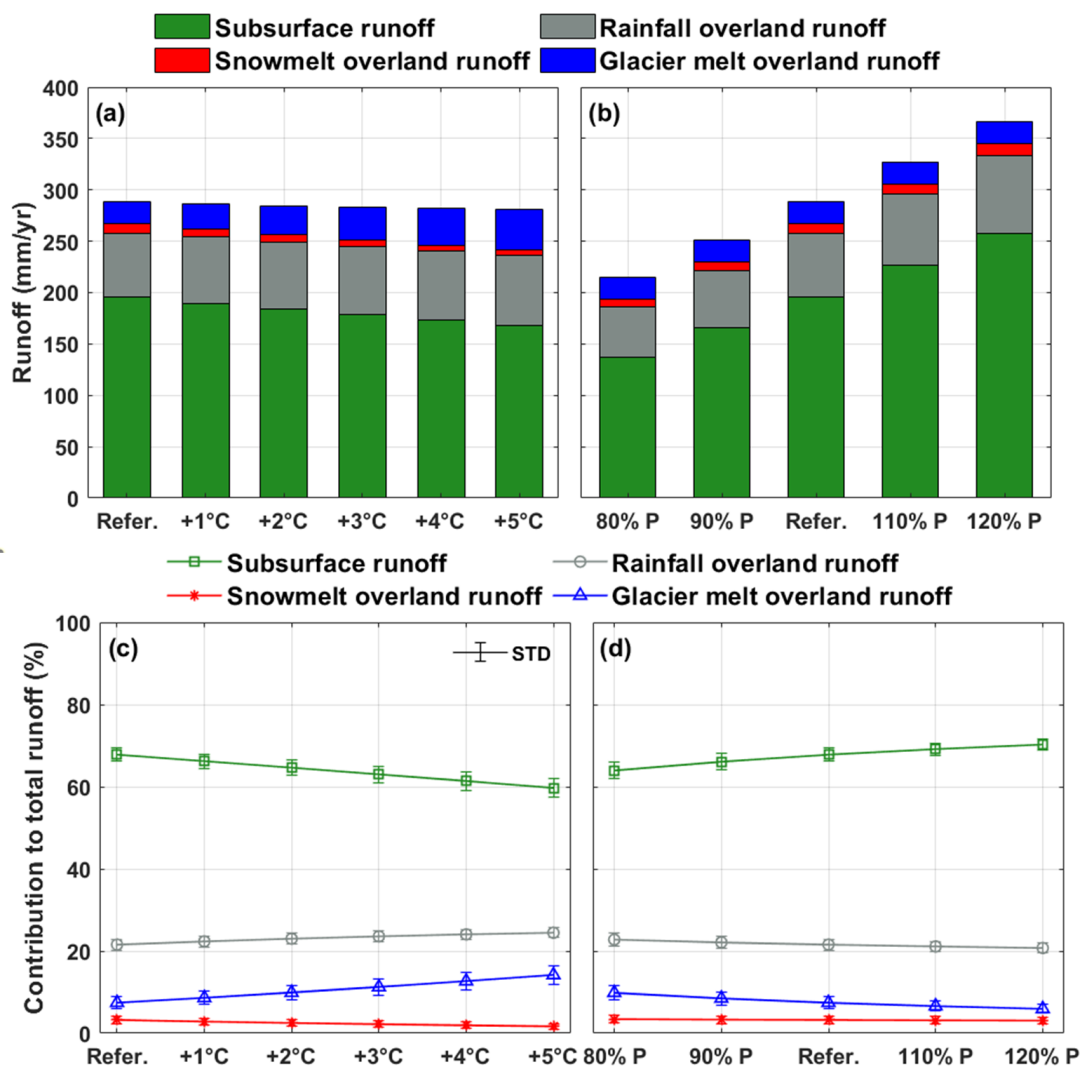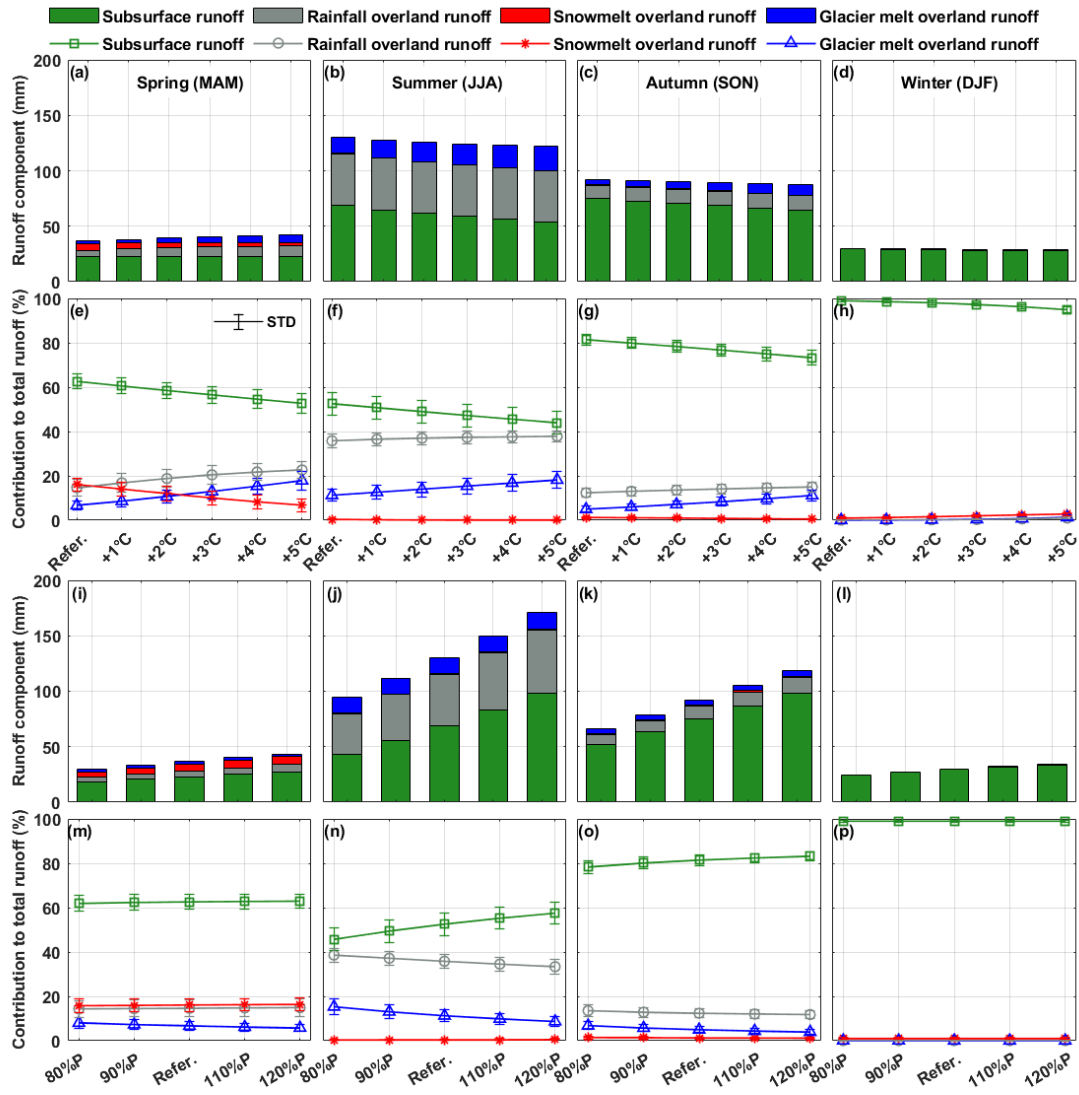

Figure 6. Sensitivities of the runoff components to perturbed temperature and precipitation. (a) and (b) amounts of runoff components, (c) and (d) contributions of runoff components to the total runoff.

With the increasing temperature, the amount and proportion of subsurface runoff decreased

20

at -5.6mm/°C and -1.6%/°C, because climate warming increased evaporation and consequently

reduced the subsurface water storage and outflow. The rainfall and snowmelt overland runoff

increased at 1.3mm/°C (0.6%/°C) and decreased at -0.9mm/°C (-0.3%/°C), respectively,

because more rainfall was partitioned from total precipitation due to higher temperature. The

glacier melt overland runoff increased significantly at 3.7mm/°C (1.4%/°C) with the increasing

temperature, and the contribution to total runoff could be around 15% for 5°C of warming. The

amount of all four runoff components increased with the increasing precipitation (Figure 6b),

with rates of 30.1mm/10%, 6.8mm/10%, 1.0mm/10% and 0.1mm/10% for subsurface, rainfall

overland, snowmelt overland and glacier melt overland runoff, respectively. However, only the

proportion of subsurface runoff increased at 1.6%/10% with the increasing precipitation, while

the proportions of three other components all decreased, with rates of -0.5%/10%, -0.1%/10%

and -1.0%/10% for rainfall overland, snowmelt overland and glacier melt overland runoff,

respectively (Figure 6d), because there was a much higher increase in the total runoff. Overall,

the contributions of runoff components were more sensitive to temperature perturbation than

precipitation perturbation.

Figure 7 and Tables S1-S4 show the runoff components in different seasons and their

sensitivities to perturbed climate. The subsurface runoff was the dominant component in all

four seasons in the reference scenario, with contribution ranging from 53% in summer to 99%

in winter. The contribution of snowmelt overland runoff was extremely low in the seasons

except for spring because of the small SCA in summer and autumn and the low temperature in

winter. The contribution of snowmelt overland runoff in spring was close to that of rainfall

overland runoff (Figure 7e-h). The contribution of glacier melt overland runoff was around half

that of rainfall overland runoff in all four seasons. With climate warming, the contribution of

subsurface runoff decreased in all four seasons, while the contributions of rainfall and glacier

melt overland runoff increased. The significantly increasing glacier melt and rainfall led to an

increase in the total runoff in spring (Figure 7a). The contribution of snowmelt overland runoff

decreased in three seasons except for winter, during which its contribution slightly increased,

and got around 3% for 5°C of warming (Figure 7h). With increasing precipitation, the amounts

of four components increased in all seasons (Figure 7i-l), but the contributions of components

remained nearly unchanged in spring, autumn and winter (Figure 7m, o-p). The contributions

of runoff components were sensitive to perturbed precipitation only in summer, during which

subsurface runoff contributed more to the runoff with increasing precipitation, while the

contributions of rainfall and glacier melt overland runoff decreased significantly (Figure 7n).

Figure 7. Sensitivities of the seasonal runoff components to perturbed temperature and

precipitation. (a)-(d) sensitivities of amounts of runoff components to perturbed temperature,

(e)-(h) sensitivities of contributions of runoff components to perturbed temperature, (i)-(l)

sensitivities of amounts of runoff components to perturbed precipitation, (m)-(p) sensitivities

of contributions of runoff components to perturbed precipitation.

**3.5 Spatial pattern of local hydrological sensitivities**

Considering that the YTR basin is a large basin with drainage area of 2×10^5 km^2, the spatial

pattern of the local hydrological sensitivity was further analyzed with the assistance of the

494   spatially distributed model structure. The runoff change at REW scale in four typical scenarios

495   (i.e., 1℃ of warming, 5℃ of warming, precipitation changing to 80% and 120%) are shown in

496   Figure 8. All REWs have the same runoff trend with the precipitation perturbation (Figure 8c

497   and 8d). The runoff increasing ranged from 12.2% to 40.4% when precipitation increased by

498   20%. In most REWs, the runoff changed at larger rates than precipitation, with few exceptions

499   located in the tributaries of Nyang River, Lhasa River and the source region of mainstream,

500   showing shallow red/blue colors in Figure 8c and 8d. On the contrary, the REW scale runoff

501   changes in response to increasing temperature had strong spatial variability (Figure 8a and 8b).

502   Although the runoff at the basin outlet decreased with climate warming, the REW scale runoff

503   increased in about half of REWs. For 5℃ of warming, the REW scale runoff changes ranged

504   from -18.6% to 54.3%. Most REWs with increasing runoff were located upstream of the

505   mainstream, the Nianchu River, the Nyang River, and the tributary of Lhasa River (Figure 8b).

506   The statistical significance of runoff change in response to climate perturbation was

507   analyzed. The runoff change in response to perturbed precipitation was significant in all the

508   REWs, but things were different for warming temperature scenarios. The number of REWs

509   with insignificant change trend decreased with the temperature warming level. In specify, the

510   runoff change was insignificant (at significance level of 0.01) in 26% and 15% area of the whole

511   basin, for the warming of 1℃ and 5℃, respectively (Figure S1). The statistical significance in

512   response to warming temperature was related to the runoff change magnitude and drainage area

513   (Figure S2). Consequently, although the runoff change at basin outlet was rather small

514   (decreasing by 0.9% and 3.4% for the warming of 1℃ and 5℃, respectively), it was still

515   statistically significant.

516   The runoff in some REWs changed non-monotonically with increasing temperature, i.e.,

517   the runoff change trend was reversed in different temperature intervals. Most of such non-

518   monotonic REWs were located in the upstream region of the mainstream, with some others

519   located in the major tributaries Nyang River, Lhasa River and Nianchu River (Figure 8e). In

520   about 75% of non-monotonic REWs, the runoff first decreased for 1℃ of warming, and then

521   changed to an increasing trend at higher warming levels, and the reserved trends occurred in

522   the other 25% of REWs. The threshold temperature of trend turning differed among non-

523   monotonic REWs, which was 3℃ in about half of the REWs. The runoff change rates in

23

524 response to increasing temperature were generally low in non-monotonic REWs, most within

525 the range of ±1%/°C.
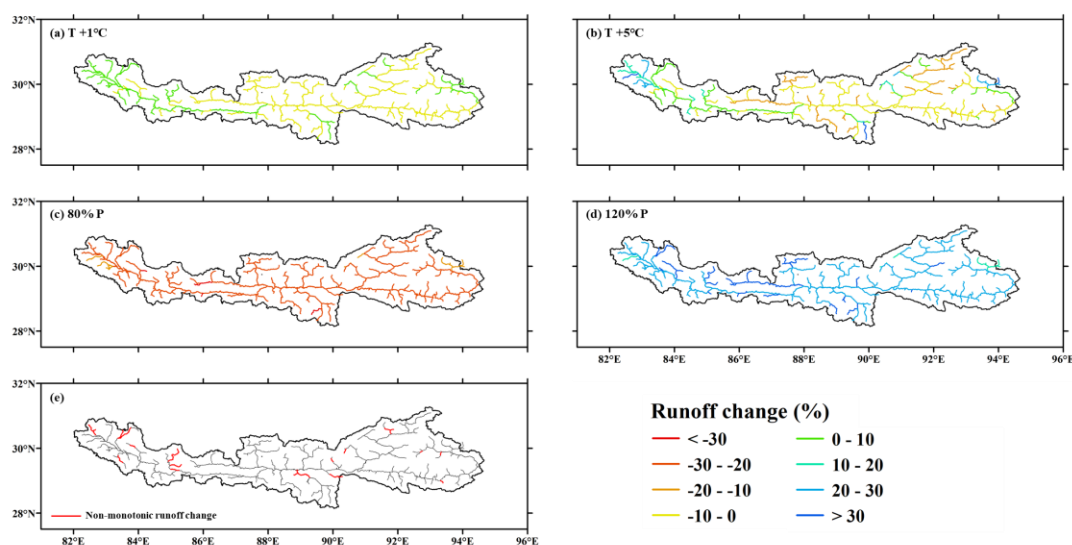
526

527 **Figure 8.** The change of REW scale runoff in response to perturbed temperature and

528 precipitation. (a) and (b) runoff change in response to temperature perturbation, (c) and (d)

529 runoff change in response to precipitation perturbation, (e) the locations of REWs showing non-

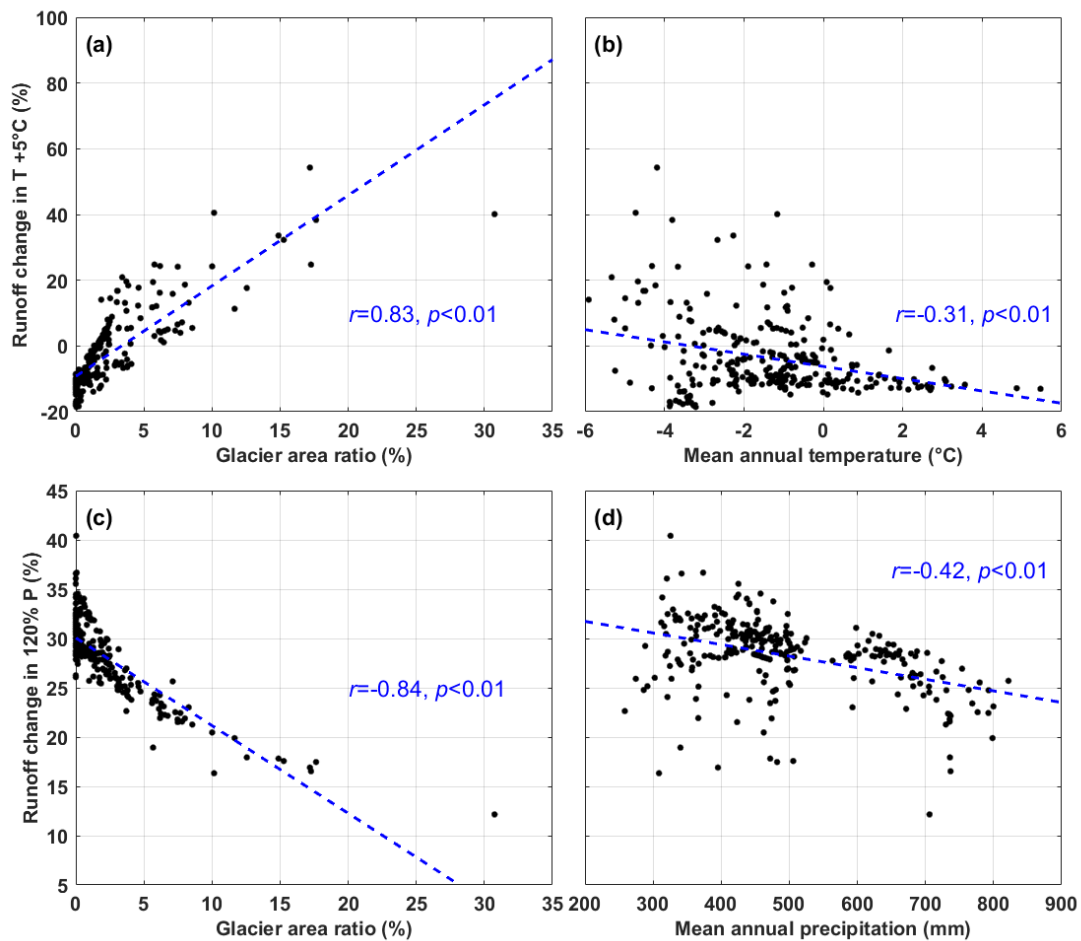530 monotonic runoff change in response to increasing temperature.

531 **4. Discussions**

532 **4.1 The influence factors of local hydrological sensitivities: the role of glaciers**

533   Our results show the strong spatial variability of the REW scale hydrological sensitivities

534 to perturbed climate. Consequently, the influence factors of the local sensitivities are analyzed

535 in this section. The basic characteristics, including mean annual temperature (MAT), mean

536 annual precipitation (MAP), average elevation (ELE), drainage area (DRA), and glacier area

537 ratio (GAR) were calculated for each REW as the potential factors. It should be noted that,

538 considering the runoff concentration processes between the upstream and downstream REWs,

539 the above characteristics were not calculated solely within each REW, but for the total drainage

540 area controlled by each REW. The correlations between the runoff change for

541 temperature/precipitation increasing by 5°C/20% and the potential influence factors were

542 analyzed. The relations with the two factors with the highest coefficients are shown in Figure

543 9. Detailed data and relations with lower coefficients are shown in Table S5 and Figure S3.

544   The GAR was the most correlated factor for the hydrological sensitivities to the

24

545   perturbation of both temperature and precipitation, with coefficients higher than 0.8 (Figure 9a

546   and 9c). The runoff change for 5°C of warming increased with the increasing GAR (Figure 9a),

547   because of the balance between the decreasing runoff caused by evaporation and the increasing

548   runoff contributed by glacier melt. In REWs where the GAR was higher than a threshold, the

549   increasing glacier melt could offset the increasing evaporation, and the runoff increased with

550   climate warming. The threshold GAR was different among REWs, ranging from 1~5%. For the

551   REWs with GAR larger than 10%, the runoff increase for 5°C of warming could be higher than

552   20%. The hydrological sensitivity to increasing temperature also had a weak but significant

553   negative correlation (r=-0.31, $p<0.01$) with the MAT of the REW (Figure 9b), which could be

554   partly attributed to the interrelation between GAR and MAT, i.e., the GAR tended to be lower

555   in warmer regions, and the runoff consequently decreased in response to increasing temperature.

556   A lower bound of runoff change could be observed in Figure 9b for the REWs with relatively

557   high MAT, again indicating the different limitation factors of evaporation, i.e., in relatively

558   warm regions, the evaporation was limited by the water condition, so increasing temperature

559   did not cause more evaporation (Wang et al., 2022).

Figure 9. The correlations between the hydrological sensitivities to climate perturbation and the dominant influence factors.

On the contrary, the runoff change in response to increasing precipitation had a significant negative correlation ($r=-0.84$, $p<0.01$) with the GAR (Figure 9c), mainly due to the spatial variability of the runoff components. In REWs with larger GAR, the contribution of precipitation-induced runoff was relatively low due to the large contribution of glacier melt runoff, thus the influence of increasing precipitation on runoff change was also small. It should be noted that based on regression line in Figure 9c, the runoff change would be around zero in regions with GAR higher than 35, which was a rather surprising inference. This might be due to the small sample of REWs with high GAR based on current spatial discretization, resulting in the poor confidence in the end of the regression line. The runoff change in response to increasing temperature also negatively correlated with the MAP ($r=-0.42$, $p<0.01$, Figure 9d). The contribution of subsurface runoff component was higher in wetter conditions (Figure 6d), resulting in more evaporation and a lower runoff coefficient, which caused a relatively small

26

575   increase in runoff, similar with the finding by He et al. (2021b).

576   Our results indicate that the runoff in some REWs changed non-monotonically in response

577   to the increasing temperature. The characteristics of these non-monotonic REWs were further

578   analyzed. Interestingly, the GAR of non-monotonic REWs had a good linear relationship with

579   their MAP (Figure 10a). The regression equation of the linear relation was

580   GAR(%)=0.011*MAP(mm)-2.43 (r=0.92). Moreover, this regression line was the dividing line

581   between the REWs where runoff increased with increasing temperature and those with opposite

582   runoff trends in the GAR-MAP plot (Figure 10a). The REWs located in the upper part of the

583   plot had larger runoff increasing rates. This indicated that the local hydrological sensitivity to

584   increasing temperature was determined by the relationship between GAR and MAP. In wetter

585   REWs with larger MAP, more glaciers were needed to offset the decreasing runoff due to the

586   increasing temperature and evaporation. These findings suggested the important role of glaciers

587   in determining the runoff change in response to climate change. Similar characteristics were

588   observed in the precipitation perturbation scenarios (Figure 10b). The runoff change rate was

589   different from the precipitation change rate in all REWs, and was consistently either higher or

590   lower than precipitation change rate in most REWs. But there were three REWs shifting from

591     $\Delta Q/\Delta P$<1 to >1, the GAR and MAP of which also had linear relationship, forming the boundary

592   of REWs where runoff changed more significantly than precipitation and those with lower

593   runoff change rate. However, there were only three such non-monotonic REWs for precipitation

594   perturbation scenarios, providing less confidence to the boundary line. As a result, there were

595   some REWs lying lower than the boundary line but with lower runoff change rate than

596   precipitation (Figure 10b).
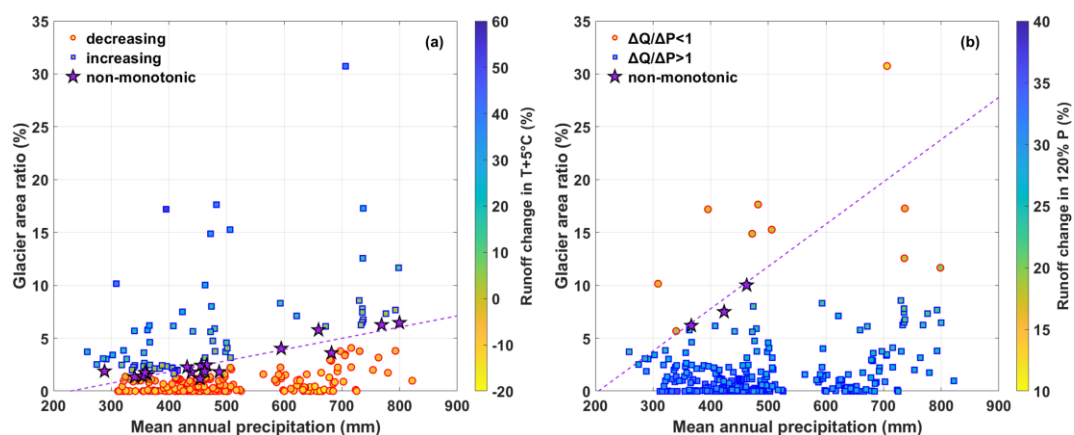
597

598   **Figure 10.** The interrelation among the REW scale glacier area ratio, mean annual

599   precipitation and the runoff change for (a) 5℃ of warming and (b) 120% precipitation.

600   **4.2 Implications of the sensitivity analysis**

601   The sensitivity analysis indicated the important role of glaciers in providing meltwater to

602   offset the runoff decreasing caused by climate warming. Our study showed that glacier

603   meltwater had a limited contribution to the total runoff in the YTR basin, similar with some

604   recent studies (Wang et al., 2021; Cui et al., 2023), resulting in a decreasing runoff trend with

605   increasing temperature. However, the spatial pattern analysis indicated that the role of glacier

606   melt runoff could be rather significant in the regions with large area covered by glaciers. For

607   example, the runoff increased significantly in the Yangbajing tributary of the Lhasa River in

608   response to increasing temperature (Figure 8), consistent with previous research estimating a

609   high contribution of glacier melt to runoff in this region (Lin et al., 2020; Wang et al., 2023). It

610   is therefore necessary to address the spatial scale issue when discussing the role of glacier

611   meltwater on water resources.

612   Several studies have stressed the important role of glaciers on the TP as the largest global

613   store of frozen water which supplied freshwater resources to downstream regions (Yao et al.,

614   2022). This study quantitively estimated the role of glacier meltwater in offsetting the

615   decreasing runoff with increasing temperature and evaporation. Our results indicated that the

616   influences of glacier on hydrological processes were highly dependent on the spatial scale and

617   the local meteorological characteristics. Specifically, the role of glacier meltwater would

618   undoubtedly be more significant in regions with larger glacier cover areas (Luo et al., 2018;

619   Zhao et al., 2019; Khanal et al., 2021). Meanwhile, the role of glaciers was smaller in wetter

620   regions with higher precipitation because of the relatively low contribution of glacier meltwater

621   in total runoff. Consequently, the regions with larger precipitation amounts but little glacier

622   coverage would face a greater risk of water resources shortage in a warming future (Figure 10a),

623   and other regions would face the similar condition because of the shrinking glacier area. Our

624   results also suggested a larger influence of precipitation change on runoff than that of

625   temperature change (Figure 4), thus an accurate projection of precipitation is crucial for the

626   assessment of water resources under climate change. Recent studies showed a decreasing

627 precipitation trend after 2000 in the YTR basin (Li et al., 2016; Luan and Zhai, 2022), likely

628 posing threats of water scarcity to the riparian regions and again highlighting the important role

629 of glacier in maintaining water resources.

630   Our results showed that the runoff responded to increasing temperature non-monotonically

631 in some regions. These non-monotonic REWs represented the most dynamic regions within the

632 basin, as they kept shifting between energy and water limited stages. Recent studies also

633 projected the non-monotonic runoff change on the TP at increasing warming levels (Cui et al.,

634 2023), i.e., the annual mean runoff for major rivers on the TP will significantly decrease by

635 0.1~3.2% at the warming level of 1.5°C, and increase by 1.5~12% at 3.0°C in the future.

636 Although seemingly similar, the two studies revealed two different phenomena. In particular,

637 the non-monotonic runoff change projected by Cui et al. (2023) was driven by the output put

638 of climatic projection data CMIP6 (Eyring et al., 2016), and the runoff change was dominated

639 by the tendencies and periodicities of climate factors, especially precipitation (Wu et al., 2022).

640 Our study analyzed the runoff change in response to climate warming with fixed precipitation

641 input, and the trend was the result of the comprehensive response of multiple water balance

642 components to climate change. The local non-monotonic hydrological sensitivity was

643 essentially a borderline condition of increasing and decreasing trend, which reflected the

644 balance of increasing meltwater and evaporation in response to climate warming.

645

4.3 Limitations

647   This study explored the sensitivities of hydrological processes to climate change by

648 designing temperature and precipitation perturbation scenarios, rather than projecting future

649 runoff using the forcing data from general circulation models (GCMs). The assumed climate

650 perturbation method is widely used in runoff projection studies (He et al., 2021b; Su et al., 2023;

651 Rasouli et al., 2014; Rasouli et al., 2015), with the advantage of avoiding the computation cost

652 of correcting biases and downscaling GCMs to regional scale (Piani et al., 2010; Xu et al.,

653 2019). However, the assumed climate perturbation did not reflect the gradual process of climate

654 change. Specifically, the temperature should go through relatively low warming levels before

655 arriving at the assumed highest level, but the climate perturbation method actually assumed an

656 abrupt climate change. Because of the relatively short simulation period, the potential trend

657 turning of meltwater caused by the combined effect of increasing melting rate and shrinking

658 glacier area cannot be reflected by the sensitivity analysis (Yao et al., 2022; Zhang et al., 2022a).

659 We can expect that the role of glaciers when temperature increases by 5℃ in the future should

660 be less than our results, because the glacier covered area at that time will be less than the current

661 condition (Yao et al., 2022). Meanwhile, the potential influences of temperature and

662 precipitation change on soil and vegetation conditions (Boulanger et al., 2016) were not

663 considered when designing the climate perturbation scenarios. Besides, because climate

664 perturbation rather than climate ensemble was used to force the model, the representation of

665 uncertainties related to climate forcing was very simplified. Nonetheless, the simple sensitivity

666 analysis in this study helped better understand the separate effect of changing temperature and

667 precipitation on runoff, and informed the role of glaciers in controlling the spatial pattern of

668 runoff change.

669 　　Another limitation comes from the uncertainties of hydrological model. Although

670 validated by the measurement data of multiple objectives and several internal stations, the

671 model still had potential uncertainties. First, as the most important forcing data, the common

672 precipitation datasets in the YTR basin all had large uncertainties, due to the lack of validation

673 data in high elevation regions (Xu et al., 2017), leading to uncertainties in hydrological

674 simulation. The model underestimated the peak streamflow for most stations, which could be

675 attributed to the underestimated precipitation during wet seasons by CMFD dataset. Further

676 correction on the precipitation product based on more station data could be helpful to remove

677 the bias. Second, because of the complex hydrological processes and runoff components, the

678 parameter equifinality problem usually existed in the hydrological model in large mountainous

679 basins (Gupta et al., 2008; Nan et al., 2021a). He et al. (2019) indicated that the uncertainties

680 of runoff component contributions could be nearly 20% even when the simulations of

681 streamflow, snow, glacier and isotope were satisfied simultaneously. The misestimation of the

682 runoff regime would undoubtedly influence the sensitivity analysis. Third, the calibration

683 procedure of this work was rather simple, based on a combination of automatic algorithm and

684 manual selection. The influences of calibration scheme, optimized objective function (Gupta et

685 al., 2009; Majone et al., 2022) and the weights of multiple objectives (Tong et al., 2021) on

686   hydrological sensitivities were not analyzed deeply. For instance, different types of evaluation

687   metrics for multiple objectives were added together directly, which may result in different

688   impacts on the integrated objective function. Besides, the use of pySOT algorithm did not allow

689   for a comprehensive hydrological uncertainty analysis, because it aimed to achieve the best

690   fitness between observations and model outputs. Lastly, the calibrated parameters were

691   assumed to be spatially uniform within the whole basin to avoid introducing too many

692   parameters. Although this is similar to several large-scale modeling studies (e.g., Cui et al.,

693   2023; Lutz et al., 2014), the uniform parameter might be inadequate to represent the spatial

694   variability of hydrological processes, which may influence some conclusions of the sensitivity

695   analysis. For example, considering the potential spatial variability of glacier melting rate, the

696   characteristics of non-monotonic REWs in Figure 10 may not form a straight line. Currently

697   this work only considered the uncertainties introduced by natural climate variabilities. More

698   works are needed in the future to analyze the parameter sensitivities and the uncertainties from

699   calibration schemes.

700   **5. Conclusions**

701   This study adopted the tracer-aided hydrological model THREW-T in a typical large

702   mountainous basin Yarlung Tsangpo River (YTR) on the Tibetan Plateau (TP). The model was

703   validated against multiple objectives (streamflow, snow, glacier and isotope) and the

704   streamflow at internal stations. The sensitivities of hydrological processes to perturbed

705   temperature and precipitation were analyzed. The spatial pattern of local hydrological

706   sensitivities and the influence factors were explored. Our main findings are as follows:

707   (1) The THREW-T model performed well on simulating the streamflow, snow cover area

708   (SCA), glacier mass balance (GMB), and stream water isotope, ensuring good representation

709   of the key cryospheric processes and a reasonable estimation of the contributions of runoff

710   components. The model performed acceptably on simulating the streamflow at eight internal

711   stations located in the mainstream and two major tributaries, which indicated that the spatial

712   pattern of hydrological processes was reflected by the model, and provided confidence in the

713   sensitivity analysis.

714   (2) Most hydrological characteristics responded to increasing temperature and

precipitation oppositely. Increasing temperature led to decreasing annual runoff, SCA and GMB, and changed the runoff variation showing a smaller inter-annual variation, a more even distributed intra-annual distribution, and an earlier maximum runoff. It also influenced the runoff regime by increasing the contributions of rainfall and glacier melt overland runoff, but decreasing the subsurface runoff and snowmelt overland runoff. Increasing precipitation had the opposite effects to increasing temperature.

(3) The distribution of local hydrological sensitivities had a strong spatial variability. The local runoff change in response to increasing temperature varied significantly, with changing rate of -18.6% to 54.3% for 5°C of warming. The glacier area ratio (GAR) was the dominant factor of the spatial pattern of hydrological sensitivities to both perturbed temperature and precipitation. Some regions had a non-monotonic runoff change rate in response to climate perturbation, which represented the most dynamic regions within the basin, as they kept shifting between energy and water limited stages. The GAR and mean annual precipitation (MAP) of the non-monotonic regions had a linear relation, and formed the boundary of regions with different runoff trends in the GAR-MAP plot.

Code and data availability

Code and data availability. The isotope data and the code of THREW-T model used in this study are available from the corresponding author (tianfq@tsinghua.edu.cn). Other data sets are publicly available as follows: DEM (http://www.gscloud.cn/sources/details/310?pid=302, last access: 1 January 2019, Geospatial Data Cloud Site, 2019), CMFD (https://doi.org/10.11888/AtmosphericPhysics.tpe.249369.file, Yang and He, 2019), glacier inventory data (https://doi.org/10.3972/glacier.001.2013.db, Liu, 2012), glacier elevation change data (https://doi.org/10.6096/13, Huggonet et al., 2021), NDVI (https://doi.org/10.5067/MODIS/MOD13A3.006, Didan, 2015), LAI (https://doi.org/10.5067/MODIS/MOD15A2H.006, Myneni et al., 2015), HWSD (https://data.tpdc.ac.cn/zh-hans/data/3519536a-d1e7-4ba1-8481-6a0b56637baf/?q=HWSD, last access: 1 January 2019, He, 2019). These datasets not publicly available are referred to in the main text (Chen et al., 2018; Liu et al., 2007).

744

Competing interests

At least one of the (co-)authors is a member of the editorial board of Hydrology and Earth System Sciences.

755

References

Aygun, O., Kinnard, C., Campeau, S., and Krogh, S. A.: Shifting Hydrological Processes in a Canadian Agroforested Catchment due to a Warmer and Wetter Climate, Water, 12, 10.3390/w12030739, 2020.

Bai, X. L., Zhao, W. Z., Liu, H., Zhang, Y. Y., Yang, Q. Y., Liu, J. T., and Chang, X. L.: Effects of precipitation changes and land-use alteration on streamflow: A comparative analysis from two adjacent catchments in the Qilian Mountains, arid northwestern China, Frontiers in Environmental Science, 11, 10.3389/fenvs.2023.1097049, 2023.

Birkel, C. and Soulsby, C.: Advancing tracer-aided rainfall-runoff modelling: a review of progress, problems and unrealised potential, Hydrological Processes, 29, 5227-5240, 10.1002/hyp.10594, 2015.

Bloschl, G. and Montanari, A.: Climate change impacts-throwing the dice?, Hydrological Processes, 24, 374-381, 10.1002/hyp.7574, 2010.

Boulanger, Y., Taylor, A. R., Price, D. T., Cyr, D., McGarrigle, E., Rammer, W., Sainte-Marie, G., Beaudoin, A., Guindon, L., and Mansuy, N.: Climate change impacts on forest landscapes along the Canadian southern boreal forest transition zone, Landscape Ecology,

32, 1415-1431, 10.1007/s10980-016-0421-7, 2017.

Cao, L. G. and Pan, S. M.: Changes in precipitation extremes over the "Three-River Headwaters" region, hinterland of the Tibetan Plateau, during 1960-2012, Quaternary International, 321, 105-115, 10.1016/j.quaint.2013.12.041, 2014.

Chen, X., Long, D., Liang, S., He, L., Zeng, C., Hao, X., and Hong, Y.: Developing a composite daily snow cover extent record over the Tibetan Plateau from 1981 to 2016 using multisource data, Remote Sensing of Environment, 215, 284-299, 10.1016/j.rse.2018.06.021, 2018.

Criss, R. E. and Winston, W. E.: Do Nash values have value? Discussion and alternate proposals, Hydrological Processes, 22, 2723-2725, 10.1002/hyp.7072, 2008.

Cui, T., Li, Y., Yang, L., Nan, Y., Li, K., Tudaji, M., Hu, H., Long, D., Shahid, M., Mubeen, A., He, Z., Yong, B., Lu, H., Li, C., Ni, G., Hu, C., and Tian, F.: Non-monotonic changes in Asian Water Towers' streamflow at increasing warming levels, Nature communications, 14, 1176-1176, 10.1038/s41467-023-36804-6, 2023.

Didan, K.: MOD13A3 MODIS/Terra vegetation Indices Monthly L3 Global 1 km SIN Grid V006, NASA EOSDIS Land Processes DAAC [dataset], https://doi.org/10.5067/MODIS/MOD13A3.006, 2015.

Eriksson, D., Bindel, D., and Shoemaker, C. A.: pySOT and POAP: An event-driven asynchronous framework for surrogate optimization, arXiv preprint, 10.48550/arXiv.1908.00420, 2019.

Eyring, V., Bony, S., Meehl, G. A., Senior, C. A., Stevens, B., Stouffer, R. J., and Taylor, K. E.: Overview of the Coupled Model Intercomparison Project Phase 6 (CMIP6) experimental design and organization, Geoscientific Model Development, 9, 1937-1958, 10.5194/gmd-9-1937-2016, 2016.

Fassnacht, S. R., Sexstone, G. A., Kashipazha, A. H., Ignacio Lopez-Moreno, J., Jasinski, M. F., Kampf, S. K., and Von Thaden, B. C.: Deriving snow-cover depletion curves for different spatial scales from remote sensing and snow telemetry data, Hydrological Processes, 30, 1708-1717, 10.1002/hyp.10730, 2016.

Fenicia, F., Kavetski, D., Reichert, P., and Albert, C.: Signature-Domain Calibration of Hydrological Models Using Approximate Bayesian Computation: Empirical Analysis of

802   Fundamental Properties, Water Resources Research, 54, 3958-3987,
803   10.1002/2017wr021616, 2018.

804   Gao, J., Yao, T. D., Masson-Delmotte, V., Steen-Larsen, H. C., and Wang, W. C.: Collapsing
805   glaciers threaten Asia's water supplies, Nature, 565, 19-21, 10.1038/d41586-018-07838-4,
806   2019.

807   Gupta, H. V., Kling, H., Yilmaz, K. K., and Martinez, G. F.: Decomposition of the mean squared
808   error and NSE performance criteria: Implications for improving hydrological modelling,
809   Journal of Hydrology, 377, 80-91, 10.1016/j.jhydrol.2009.08.003, 2009.

810   Gupta, H. V., Wagener, T., and Liu, Y.: Reconciling theory with observations: elements of a
811   diagnostic approach to model evaluation, Hydrological Processes, 22, 3802-3813,
812   10.1002/hyp.6989, 2008.

813   He, Y.: Pan-TPE soil map based on Harmonized World Soil Database (V1.2), National Tibetan
814   Plateau Data Center [dataset], 2019.

815   He, Z. H. and Pomeroy, J. W.: Assessing hydrological sensitivity to future climate change over
816   the Canadian southern boreal forest, Journal of Hydrology, 624,
817   10.1016/j.jhydrol.2023.129897, 2023.

818   He, Z., Duethmann, D., and Tian, F.: A meta-analysis based review of quantifying the
819   contributions of runoff components to streamflow in glacierized basins, Journal of
820   Hydrology, 603, 10.1016/j.jhydrol.2021.126890, 2021a.

821   He, Z. H., Pomeroy, J. W., Fang, X., and Peterson, A.: Sensitivity analysis of hydrological
822   processes to perturbed climate in a southern boreal forest basin, Journal of Hydrology, 601,
823   10.1016/j.jhydrol.2021.126706, 2021b.

824   He, Z., Unger-Shayesteh, K., Vorogushyn, S., Weise, S. M., Kalashnikova, O., Gafurov, A.,
825   Duethmann, D., Barandun, M., and Merz, B.: Constraining hydrological model parameters
826   using water isotopic compositions in a glacierized basin, Central Asia, Journal of
827   Hydrology, 571, 332-348, 10.1016/j.jhydrol.2019.01.048, 2019.

828   Hindshaw, R. S., Tipper, E. T., Reynolds, B. C., Lemarchand, E., Wiederhold, J. G., Magnusson,
829   J., Bernasconi, S. M., Kretzschmar, R., and Bourdon, B.: Hydrological control of stream
830   water chemistry in a glacial catchment (Damma Glacier, Switzerland), Chemical Geology,
831   285, 215-230, 10.1016/j.chemgeo.2011.04.012, 2011.

832 Hugonnet, R., McNabb, R., Berthier, E., Menounos, B., Nuth, C., Girod, L., Farinotti, D., Huss,

833   M., Dussaillant, I., Brun, F., and Kaab, A.: Accelerated global glacier mass loss in the early

834   twenty-first century, Nature, 592, 726-+, 10.1038/s41586-021-03436-z, 2021.

835 Immerzeel, W. W., van Beek, L. P. H., and Bierkens, M. F. P.: Climate Change Will Affect the

836   Asian Water Towers, Science, 328, 1382-1385, 10.1126/science.1183188, 2010.

837 Jiang, Y., Xu, Z., and Xiong, L.: Runoff variation and response to precipitation on multi-spatial

838   and temporal scales in the southern Tibetan Plateau, Journal of Hydrology-Regional

839   Studies, 42, 10.1016/j.ejrh.2022.101157, 2022a.

840 Jiang, Y., Yang, K., Yang, H., Lu, H., Chen, Y., Zhou, X., Sun, J., Yang, Y., and Wang, Y.:

841   Characterizing basin-scale precipitation gradients in the Third Pole region using a high-

842   resolution atmospheric simulation-based dataset, Hydrology and Earth System Sciences,

843   26, 4587-4601, 10.5194/hess-26-4587-2022, 2022b.

844 Khanal, S., Lutz, A. F., Kraaijenbrink, P. D. A., van den Hurk, B., Yao, T., and Immerzeel, W.

845   W.: Variable 21st Century Climate Change Response for Rivers in High Mountain Asia at

846   Seasonal to Decadal Time Scales, Water Resources Research, 57, 10.1029/2020wr029266,

847   2021.

848 Li, X., Yao, Z., Xiao, J., and Wang, H.: Analysis of the spatial-temporal variation characteristics

849   of precipitation over the Tibetan Plateau from 1961 through 2010, Journal of Glaciology

850   and Geocryology, 38, 1233-1240, 2016.

851 Li, C., Sinha, E., Horton, D. E., Diffenbaugh, N. S., and Michalak, A. M.: Joint bias correction

852   of temperature and precipitation in climate model simulations, Journal of Geophysical

853   Research-Atmospheres, 119, 13153-13162, 10.1002/2014jd022514, 2014.

854 Li, Z. X., Feng, Q., Li, Z. J., Yuan, R. F., Gui, J., and Lv, Y. M.: Climate background, fact and

855   hydrological effect of multiphase water transformation in cold regions of the Western

856   China: A review, Earth-Science Reviews, 190, 33-57, 10.1016/j.earscirev.2018.12.004,

857   2019.

858 Li, Z. J., Li, Z. X., Song, L. L., Gui, J., Xue, J., Zhang, B. J., and Gao, W. D.: Hydrological and

859   runoff formation processes based on isotope tracing during ablation period in the source

860   regions of Yangtze River, Hydrology and Earth System Sciences, 24, 4169-4187,

861   10.5194/hess-24-4169-2020, 2020.

862 Li, K., Tian, F., Khan, M. Y. A., Xu, R., He, Z., Yang, L., Lu, H., and Ma, Y.: A high-accuracy

863   rainfall dataset by merging multiple satellites and dense gauges over the southern Tibetan

864   Plateau for 2014-2019 warm seasons, Earth System Science Data, 13, 5455-5467,

865   10.5194/essd-13-5455-2021, 2021.

866 Lin, L., Gao, M., Liu, J., Wang, J., Wang, S., Chen, X., and Liu, H.: Understanding the effects

867   of climate warming on streamflow and active groundwater storage in an alpine catchment:

868   the upper Lhasa River, Hydrology and Earth System Sciences, 24, 1145-1157,

869   10.5194/hess-24-1145-2020, 2020.

870 Liu, S.: The second glacier inventory dataset of China (version 1.0) (2006–2011), National

871   Tibetan Plateau Data Center [dataset], 10.3972/glacier.001.2013.db, 2012.

872 Liu, Z. F., Tian, L. D., Yao, T. D., Gong, T. L., Yin, C. L., and Yu, W. S.: Temporal and spatial

873   variations of delta O-18 in precipitation of the Yarlung Zangbo River Basin, Journal of

874   Geographical Sciences, 17, 317-326, 10.1007/s11442-007-0317-1, 2007.

875 Luan, L. and Zhai, P.: Changes in rainy season precipitation properties over the Qinghai-Tibet

876   Plateau based on multi-source datasets, Progressus Inquisitiones de Mutatione Climatis,

877   19, 173-190, 2023.

878 Luo, Y., Arnold, J., Liu, S., Wang, X., and Chen, X.: Inclusion of glacier processes for

879   distributed hydrological modeling at basin scale with application to a watershed in

880   Tianshan Mountains, northwest China, Journal of Hydrology, 477, 72-85,

881   10.1016/j.jhydrol.2012.11.005, 2013.

882 Luo, Y., Arnold, J., Liu, S. Y., Wang, X. Y., and Chen, X.: Inclusion of glacier processes for

883   distributed hydrological modeling at basin scale with application to a watershed in

884   Tianshan Mountains, northwest China, Journal of Hydrology, 477, 72-85,

885   10.1016/j.jhydrol.2012.11.005, 2013.

886 Luo, Y., Wang, X., Piao, S., Sun, L., Ciais, P., Zhang, Y., Ma, C., Gan, R., and He, C.:

887   Contrasting streamflow regimes induced by melting glaciers across the Tien Shan - Pamir

888   - North Karakoram, Scientific Reports, 8, 10.1038/s41598-018-34829-2, 2018.

889 Luo, Y., Wang, X. L., Piao, S. L., Sun, L., Ciais, P., Zhang, Y. Q., Ma, C. K., Gan, R., and He,

890   C. S.: Contrasting streamflow regimes induced by melting glaciers across the Tien Shan -

891   Pamir - North Karakoram, Scientific Reports, 8, 10.1038/s41598-018-34829-2, 2018.

892 Lutz, A. F., Immerzeel, W. W., Shrestha, A. B., and Bierkens, M. F. P.: Consistent increase in

893   High Asia's runoff due to increasing glacier melt and precipitation, Nature Climate Change,

894   4, 587-592, 10.1038/nclimate2237, 2014.

895 Majone, B., Avesani, D., Zulian, P., Fiori, A., and Bellin, A.: Analysis of high streamflow

896   extremes in climate change studies: how do we calibrate hydrological models?, Hydrology

897   and Earth System Sciences, 26, 3863-3883, 10.5194/hess-26-3863-2022, 2022.

898 McMillan, H., Westerberg, I., and Branger, F.: Five guidelines for selecting hydrological

899   signatures, Hydrological Processes, 31, 4757-4761, 10.1002/hyp.11300, 2017.

900 Moriasi, D. N., Arnold, J. G., Van Liew, M. W., Bingner, R. L., Harmel, R. D., and Veith, T. L.:

901   Model evaluation guidelines for systematic quantification of accuracy in watershed

902   simulations, Transactions of the Asabe, 50, 885-900, 10.13031/2013.23153, 2007.

903 Myneni, R., Knyazikhin, Y., and Park, T.: MOD15A2H MODIS/Terra Leaf Area Index/FPAR

904   8-Day L4 Global 500 m SIN Grid V006, NASA EOSDIS Land Processes DAAC [dataset],

905   10.5067/MODIS/MOD15A2H.006, 2015.

906 Nan, Y., Tian, F., Li, Z., and Gui, J.: Longer simulation time step of the tracer-aided hydrological

907   model estimates lower contribution of slow runoff components, Journal of Hydrology,

908   https://doi.org/10.1016/j.jhydrol.2023.129889, 2023.

909 Nan, Y., He, Z., Tian, F., Wei, Z., and Tian, L.: Can we use precipitation isotope outputs of

910   isotopic general circulation models to improve hydrological modeling in large

911   mountainous catchments on the Tibetan Plateau?, Hydrology and Earth System Sciences,

912   25, 6151-6172, 10.5194/hess-25-6151-2021, 2021a.

913 Nan, Y., He, Z., Tian, F., Wei, Z., and Tian, L.: Assessing the influence of water sampling

914   strategy on the performance of tracer-aided hydrological modeling in a mountainous basin

915   on the Tibetan Plateau, Hydrology and Earth System Sciences, 26, 4147-4167,

916   10.5194/hess-26-4147-2022, 2022.

917 Nan, Y., Tian, L., He, Z., Tian, F., and Shao, L.: The value of water isotope data on improving

918   process understanding in a glacierized catchment on the Tibetan Plateau, Hydrology and

919   Earth System Sciences, 25, 3653-3673, 10.5194/hess-25-3653-2021, 2021b.

920 Olsson, T., Jakkila, J., Veijalainen, N., Backman, L., Kaurola, J., and Vehvilainen, B.: Impacts

921   of climate change on temperature, precipitation and hydrology in Finland - studies using

bias corrected Regional Climate Model data, Hydrology and Earth System Sciences, 19, 3217-3238, 10.5194/hess-19-3217-2015, 2015.

Piani, C., Weedon, G. P., Best, M., Gomes, S. M., Viterbo, P., Hagemann, S., and Haerter, J. O.: Statistical bias correction of global simulated daily precipitation and temperature for the application of hydrological models, Journal of Hydrology, 395, 199-215, 10.1016/j.jhydrol.2010.10.024, 2010.

Rasouli, K., Pomeroy, J. W., and Marks, D. G.: Snowpack sensitivity to perturbed climate in a cool mid-latitude mountain catchment, Hydrological Processes, 29, 3925-3940, 10.1002/hyp.10587, 2015.

Rasouli, K., Pomeroy, J. W., Janowicz, J. R., Carey, S. K., and Williams, T. J.: Hydrological sensitivity of a northern mountain basin to climate change, Hydrological Processes, 28, 4191-4208, 10.1002/hyp.10244, 2014.

Reggiani, P., Hassanizadeh, S. M., Sivapalan, M., and Gray, W. G.: A unifying framework for watershed thermodynamics: constitutive relationships, Advances in Water Resources, 23, 15-39, 10.1016/s0309-1708(99)00005-6, 1999.

Schaefli, B. and Gupta, H. V.: Do Nash values have value?, Hydrological Processes, 21, 99-104, 2007.

Schaefli, B., Hingray, B., Niggli, M., and Musy, A.: A conceptual glacio-hydrological model for high mountainous catchments, Hydrology and Earth System Sciences, 9, 95-109, 10.5194/hess-9-95-2005, 2005.

Stadnyk, T. A. and Holmes, T. L.: Large scale hydrologic and tracer aided modelling: A review, Journal of Hydrology, 618, 10.1016/j.jhydrol.2023.129177, 2023.

Su, T., Miao, C. Y., Duan, Q. Y., Gou, J. J., Guo, X. Y., and Zhao, X.: Hydrological response to climate change and human activities in the Three-River Source Region, Hydrology and Earth System Sciences, 27, 1477-1492, 10.5194/hess-27-1477-2023, 2023.

Tang, Q. H., Lan, C., Su, F. G., Liu, X. C., Sun, H., Ding, J., Wang, L., Leng, G. Y., Zhang, Y. Q., Sang, Y. F., Fang, H. Y., Zhang, S. F., Han, D. M., Liu, X. M., He, L., Xu, X. M., Tang, Y., and Chen, D. L.: Streamflow change on the Qinghai-Tibet Plateau and its impacts, Chinese Science Bulletin-Chinese, 64, 2807-2821, 10.1360/tb-2019-0141, 2019.

Tian, F., Hu, H., Lei, Z., and Sivapalan, M.: Extension of the Representative Elementary

952   Watershed approach for cold regions via explicit treatment of energy related processes,

953   Hydrology and Earth System Sciences, 10, 619-644, 10.5194/hess-10-619-2006, 2006.

954 Tian, F., Xu, R., Nan, Y., Li, K., and He, Z.: Quantification of runoff components in the Yarlung

955   Tsangpo River using a distributed hydrological model, Advances in Water Science, 31,

956   324-336, 2020.

957 Tong, R., Parajka, J., Salentinig, A., Pfeil, I., Komma, J., Szeles, B., Kuban, M., Valent, P.,

958   Vreugdenhil, M., Wagner, W., and Bloeschl, G.: The value of ASCAT soil moisture and

959   MODIS snow cover data for calibrating a conceptual hydrologic model, Hydrology and

960   Earth System Sciences, 25, 1389-1410, 10.5194/hess-25-1389-2021, 2021.

961 van Pelt, S. C., Kabat, P., ter Maat, H. W., van den Hurk, B., and Weerts, A. H.: Discharge

962   simulations performed with a hydrological model using bias corrected regional climate

963   model input, Hydrology and Earth System Sciences, 13, 2387-2397, 10.5194/hess-13-

964   2387-2009, 2009.

965 van Pelt, S. C., Kabat, P., ter Maat, H. W., van den Hurk, B. J. J. M., and Weerts, A. H.:

966   Discharge simulations performed with a hydrological model using bias corrected regional

967   climate model input, Hydrology and Earth System Sciences, 13, 2387-2397, 10.5194/hess-

968   13-2387-2009, 2009.

969 Wang, S., Liu, J., Pritchard, H. D., Ke, L., Qiao, X., Zhang, J., Xiao, W., and Zhou, Y.:

970   Characterizing 4 decades of accelerated glacial mass loss in the west Nyainqentanglha

971   Range of the Tibetan Plateau, Hydrology and Earth System Sciences, 27, 933-952,

972   10.5194/hess-27-933-2023, 2023.

973 Wang, T., Zhao, Y. T., Xu, C. Y., Ciais, P., Liu, D., Yang, H., Piao, S. L., and Yao, T. D.:

974   Atmospheric dynamic constraints on Tibetan Plateau freshwater under Paris climate

975   targets, Nature Climate Change, 11, 10.1038/s41558-020-00974-8, 2021.

976 Wang, Y. W., Wang, L., Zhou, J., Yao, T. D., Yang, W., Zhong, X. Y., Liu, R. S., Hu, Z. D., Luo,

977   L., Ye, Q. H., Chen, N. S., and Ding, H. T.: Vanishing Glaciers at Southeast Tibetan Plateau

978   Have Not Offset the Declining Runoff at Yarlung Zangbo, Geophysical Research Letters,

979   48, 10.1029/2021gl094651, 2021.

980 Wang, L., Han, S., Tian, F., Li, K., Li, Y., Tudaji, M., Cao, X., Nan, Y., Cui, T., Zheng, X., Hu,

981   Z., Wang, W., and Yang, Y.: The Evaporation on the Tibetan Plateau Stops Increasing in

the Recent Two Decades, Journal of Geophysical Research-Atmospheres, 127, 10.1029/2022jd037377, 2022.

Wang, L., Yao, T. D., Chai, C. H., Cuo, L., Su, F. G., Zhang, F., Yao, Z. J., Zhang, Y. S., Li, X. P., Qi, J., Hu, Z. D., Liu, J. S., and Wang, Y. W.: TP-River: Monitoring and Quantifying Total River Runoff from the Third Pole, Bulletin of the American Meteorological Society, 102, E948-E965, 10.1175/bams-d-20-0207.1, 2021.

Wu, Y., Long, D., Lall, U., Scanlon, B. R., Tian, F., Fu, X., Zhao, J., Zhang, J., Wang, H., and Hu, C.: Reconstructed eight-century streamflow in the Tibetan Plateau reveals contrasting regional variability and strong nonstationarity, Nature Communications, 13, 10.1038/s41467-022-34221-9, 2022.

Xu, R., Hu, H. C., Tian, F. Q., Li, C., and Khan, M. Y. A.: Projected climate change impacts on future streamflow of the Yarlung Tsangpo-Brahmaputra River, Global and Planetary Change, 175, 144-159, 10.1016/j.gloplacha.2019.01.012, 2019.

Xu, R., Tian, F., Yang, L., Hu, H., Lu, H., and Hou, A.: Ground validation of GPM IMERG and TRMM 3B42V7 rainfall products over southern Tibetan Plateau based on a high-density rain gauge network, Journal of Geophysical Research-Atmospheres, 122, 910-924, 10.1002/2016jd025418, 2017.

Yang, K. and He, J.: China meteorological forcing dataset (1979–2018), National Tibetan Plateau Data Center [dataset], 10.11888/AtmosphericPhysics.tpe.249369.file, 2019.

Yao, T. D.: Tackling on environmental changes in Tibetan Plateau with focus on water, ecosystem and adaptation, Science Bulletin, 64, 417-417, 10.1016/j.scib.2019.03.033, 2019.

Yao, Y. Y., Zheng, C. M., Andrews, C. B., Scanlon, B. R., Kuang, X. X., Zeng, Z. Z., Jeong, S. J., Lancia, M., Wu, Y. P., and Li, G. S.: Role of Groundwater in Sustaining Northern Himalayan Rivers, Geophysical Research Letters, 48, 10.1029/2020gl092354, 2021.

Yao, T. D., Bolch, T., Chen, D. L., Gao, J., Immerzeel, W., Piao, S., Su, F. G., Thompson, L., Wada, Y., Wang, L., Wang, T., Wu, G. J., Xu, B. Q., Yang, W., Zhang, G. Q., and Zhao, P.: The imbalance of the Asian water tower, Nature Reviews Earth & Environment, 3, 618-632, 10.1038/s43017-022-00299-4, 2022.

Yoshimura, K., Kanamitsu, M., Noone, D., and Oki, T.: Historical isotope simulation using

1012   Reanalysis atmospheric data, Journal of Geophysical Research-Atmospheres, 113,

1013   10.1029/2008jd010074, 2008.

1014   Zhang, T., Li, D., East, A. E., Walling, D. E., Lane, S., Overeem, I., Beylich, A. A., Koppes, M.,

1015   and Lu, X.: Warming-driven erosion and sediment transport in cold regions, Nature

1016   Reviews Earth & Environment, 3, 832-851, 10.1038/s43017-022-00362-0, 2022a.

1017   Zhang, T., Li, D. F., and Lu, X. X.: Response of runoff components to climate change in the

1018   source-region of the Yellow River on the Tibetan plateau, Hydrological Processes, 36,

1019   10.1002/hyp.14633, 2022b.

1020   Zhang, F., Zhang, H. B., Hagen, S. C., Ye, M., Wang, D. B., Gui, D. W., Zeng, C., Tian, L. D.,

1021   and Liu, J. S.: Snow cover and runoff modelling in a high mountain catchment with scarce

1022   data: effects of temperature and precipitation parameters, Hydrological Processes, 29, 52-

1023   65, 10.1002/hyp.10125, 2015.

1024   Zhao, Q., Ding, Y., Wang, J., Gao, H., Zhang, S., Zhao, C., Xu, J., Han, H., and Shangguan, D.:

1025   Projecting climate change impacts on hydrological processes on the Tibetan Plateau with

1026   model calibration against the glacier inventory data and observed streamflow, Journal of

1027   Hydrology, 573, 60-81, 10.1016/j.jhydrol.2019.03.043, 2019.